Supplementary Information

Discrete oligourethanes of sequence-regulated properties – impact of stereocontrol

Weronika Forysiak,[a, b] Sara Kozub,[a] Łukasz John[b] and Roza Szweda*[a]

[a] *Łukasiewicz Research Network – PORT Polish Center for Technology Development, ul. Stabłowicka 147, 54-066 Wrocław, Poland. *Email: Roza.Szweda@port.lukasiewicz.gov.pl*

[b] *Faculty of Chemistry, University of Wrocław, 14 F. Joliot-Curie, 50-383 Wrocław, Poland.*

Abstract: Properties and functions of natural biopolymers such as proteins are strongly dependent on the sequence of amino acid monomers. The regulation of the properties of synthetic polymers by controlling monomer composition and order in macromolecule chains is a very intriguing approach that has not been thoroughly investigated so far. It is not understood to which extent we can control the properties of synthetic macromolecules by changing their sequence and stereochemistry. Moreover, compared to classical polymerization protocol, a multistep synthesis leading to perfectly sequence-defined macromolecules has many restrictions. The synthesis limitations inhibit studies of the properties and applications of sequence-defined macromolecules. Here, we investigated oligourethane models to learn about a sequence-property relationship and how stereocontrol can influence their characteristics. We have simplified the solution synthesis protocol by limiting purification steps; therefore, the oligomers can be obtained on a large scale, with good yield and high purity. We found that monomer sequence composition can be used as a tool for regulating the thermal properties of oligourethanes and can influence the degradation pathway. By inducing chirality into macromolecules we can precisely program hydrodynamic volume, thermal characteristics, and optical activity.

Table of Contents

I. Experimental Procedures

A. Materials and chemicals

3-amino-1-propanol (A, 99%, TCI) , 3-(aminomethyl)benzyl alcohol (C, 97%, Ambeed), (S)-2-amino-1-propanol (B, 98%, Apollo Scientific, ee: 97%, optical rotation: [α]20/D +18°), N,N'-disuccinimidyl carbonate (dSU, >98%, TCI), pyridine (99.8%, anhydrous, Sigma-Aldrich), anisole (99%, Alfa Aesar), acetonitrile (99.8%, anhydrous, Sigma-Aldrich), dichloromethane (DCM, >99.8%, Honeywell), ethyl acetate (99.5%,Chemsolute), sodium chloride (≥ 99.5%, Sigma-Aldrich), were used as received from the suppliers. Benzyl alcohol (Bz, 98%, Chempur) was distilled under reduced pressure before use.

B. Synthesis of oligomers

1. General description of the synthesis procedure

Sequence-defined oligocarbamates (OU1-OU10) were synthesized via liquid-phase synthesis. The first step of the synthesis is the initiation step – activation of the hydroxyl group of the benzyl alcohol using N,N'-disuccinimidyl carbonate – activator (Scheme S1 a). The products of this reaction are N-succinimidyl carbonate (activated alcohol) and N-hydroxysuccinimid by-product. The propagation consists of two steps: (I) chemoselective coupling of amino alcohol – monomer to N-succinimidyl carbonate (Scheme S1 b) and (II) activation of hydroxyl end-group of growing chain by adding N,N'-disuccinimidyl carbonate – activator. Steps I and II are performed in one-pot. After the full conversion of monomer coupling, to remove the N-hydroxysuccinimide by-product, an extraction (water/ethyl acetate) was performed. The organic phase was dried with anhydrous magnesium sulfate, filtered, and the solvent was evaporated. The flask was kept under a vacuum for one hour to dry the oligomer thoroughly. The described steps of activation, coupling and extraction were repeated cyclically until the desired oligomer was formed.

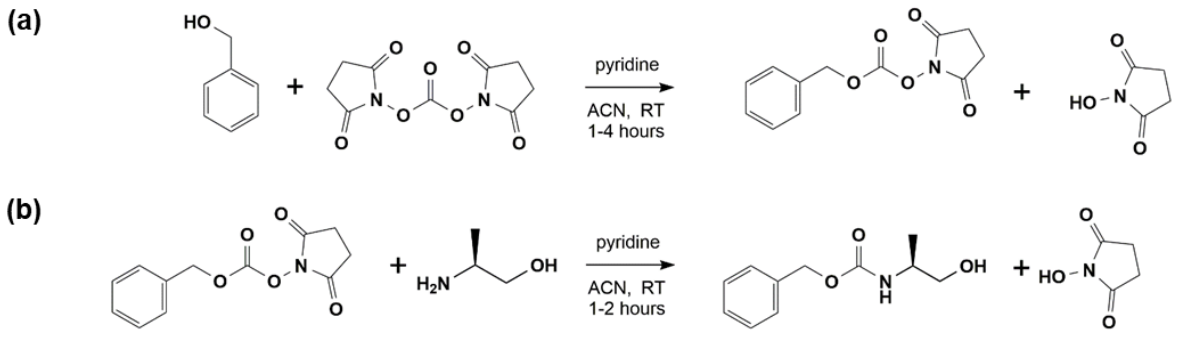

Scheme S1. Solution synthesis of sequence—defined oligomer.

The difference in the polarity between carbonate and hydroxy terminated oligomers enables convenient monitoring of the course of reactions by HPLC (Fig. S1). The exact time for activation differs

between sequences and it takes 1-4 hours, whereas, the coupling reaction is faster and takes 30-60 minutes. The amount of used reagents for synthesis OU1-OU10 summarizes Table S1. Stepwise and overall yields are calculated gravimetrically and listed in Table S2. The purity of crude oligomers OU1-OU10 was determined by HPLC (Table S3).

2. Synthesis of OU1 (Bz-AAAA)

N,N'-disuccinimidyl carbonate (568 mg, 2.22 mmol) was weighed into a 50 mL flask with a magnetic stirrer and closed with a rubber septum. The reaction vessel was degassed to remove air and filled with an inert atmosphere (N_2). After the flask was disconnected from the nitrogen vacuum line, 6 mL of anhydrous acetonitrile, 192 µL of distilled benzyl alcohol (200 mg, 1.85 mmol), and 5 µL of anisole as standard were added sequentially. Next, 449 µl of pyridine (439 mg, 5.55 mmol) was added. The mixture was stirred at room temperature, and RP-HPLC analyses were performed after every 30 minutes to estimate the conversion of benzyl alcohol to the activated form. After confirming complete substrate conversion to product, 200 µl of monomer A, 3-amino-1-propanol (166.7 mg, 2.22 mmol), was added. RP-HPLC analyses were performed every 30 minutes to estimate if all activated benzyl alcohol had reacted with the monomer. After confirming the completion of the coupling reaction, the acetonitrile was removed using a rotary evaporator (40 °C). Next, an extraction was performed to remove the side product – N-hydroxysuccinimide (Su-OH). Su-OH was formed after each activation and coupling step from N,N'-disuccinimidyl carbonate (dSu). Extraction was carried out with ethyl acetate (20 mL) and brine (10 mL). The organic phase, containing the product was dried with anhydrous Na_2SO_4. Afterwards, the mixture was filtered and the solvent was removed at 40 ^oC under reduced pressure using a rotary evaporator. Next, the obtained Bz-A oligomer was activated and coupled with another monomer according to the procedure described above. The synthesis steps were repeated until the Bz-AAAA tetramer was obtained.

The reaction time for each step was estimated based on RP-HPLC monitoring (Fig. S1). During the activation stage, the disappearance of the signal from the substrate with a free hydroxyl group was observed at approx. 8-10 minutes of retention time. During monomer coupling, to confirm the completion of the reaction, the signal from the activated carbonate at approx. 12-13 minutes of retention time was expected to disappear. HPLC monitoring allowed to establish the optimal reaction times to achieve full conversion. Figure S1A presents the chromatograms showing the course of individual reactions on the example of the Bz-BBAA oligomer synthesis.

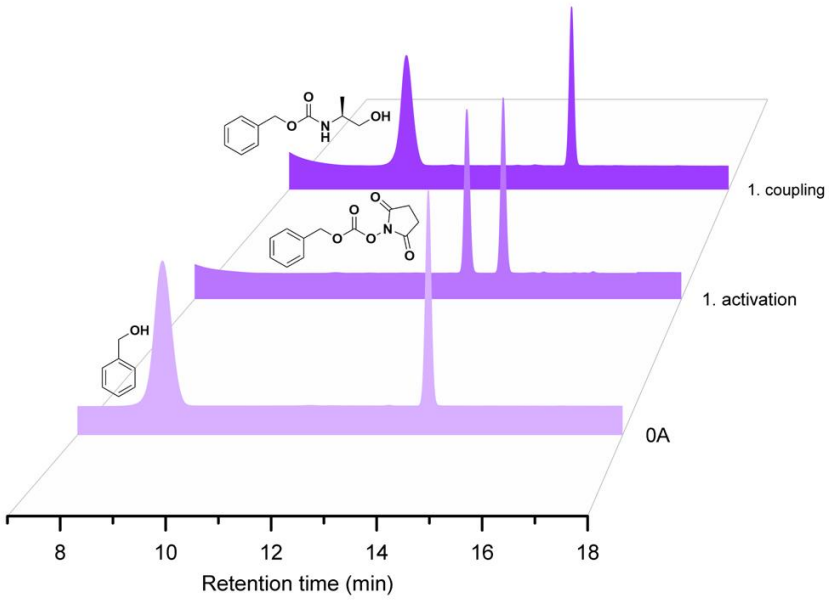

Figure S1. HPLC monitoring of the first cycle of the synthesis of Bz-BBAA (signal at 14 min is coming from anisole reference).

II. Methods

A. Nuclear Magnetic Resonance (NMR)

^{1}H NMR spectra of oligomers were recorded in deuterated chloroform (99.8 atom % D, Sigma Aldrich) using Avance III HD 500 MHZ NMR Spectrometer (BRUKER) equipped with probes: BBI and BBO. The recorded spectra were calibrated according to the chloroform signal (7.26 ppm) and evaluated in MNova software.

B. Ultra-High Performance Liquid Chromatography (HPLC)

The Reverse Phase Ultra High-Performance Liquid Chromatography (RP-UHPLC) was used for monitoring solution synthesis. Analyses were performed using Thermo Scientific Dionex UltiMate 3000 with vacuum degasser SRD-3200, two-component quaternary pump, autosampler UltiMate™ WPS-3000SL/TSL, column thermostat TCC-3000SD, and diode array detector DAD-3000. The system was equipped with a reverse-phase Hypersil Gold C18 (150x4.6mm 5u Hypersil GOLD) column with a column guard. The chromatograms were recorded in the λ=190-400 nm range. Experimental conditions: phase A: 10% ACN (HPLC grade, ≥99.9%, Honeywell) in water (MiliQ), phase B: 10% ACN (HPLC grade, ≥99.9%, Honeywell); gradient elution: -1-0 min 10% B, 0-15 min 10-100%B, 15-18 min 100%B, 18-20 min 100-10% B; flow rate: 0.5 mL·min^{-1}; T=25 ^{o}C. The chromatograms were analyzed at 220 nm using Chromeleon software. The purity of oligomers OU1-OU10 was calculated by the peak integration in the time range of 8-14 min for samples measured in acetonitrile in the Chromeleon software.

C. Liquid Chromatography - Mass Spectrometry (LC-MS)

For all LC-MS measurements, water (phase A, LC-MS grade, Merck) and acetonitrile (ACN, phase B, LC-MS grade, Merck) with 0,1% formic acid (FA, 99-100%, VWR) were used as mobile phases. For LC-MS/MS analyzes, the oligourethane samples were dissolved in a water:acetonitrile (H_2O:ACN) mixture. The resulting stock solutions had a concentration of 2 mg/ml or 5 mg/ml. The stock solutions were then diluted to a final concentration of 50 µg/ml with a 1:1 H_2O:ACN solution containing 0.1% formic acid. 2 µl of each diluted sample was used for injection onto the LC column.

The measurements were performed on a high-resolution Q-ToF spectrometer (Bruker Daltonics, Germany) equipped with an electrospray ionization (ESI) source connected to Dionex UltiMate 3000 RSLC (Thermo Scientific, USA) ultrahigh-performance liquid chromatography system. The chromatographic separations were carried out on Syncronis C18 100 x 2.1 mm × 1.7 µm column (Thermo Scientific) in a gradient mode with a column oven set to 40°C. Mobile phase A was 0.1% FA in water and mobile phase B was 0.1% FA in ACN. The gradient started with 5% of mobile phase B, and was held on 5% B for 1 min, reached 80% B in 21 min, and 95% B in 21.5 min, was held on 95% B for

another 5 min, and in the end, the column was stabilized on 5% B for another 3 min. In addition to MS detection, UV-DAD in 220 nm and 260 nm wavelengths were performed.

The spectrometer operated in automatic MS/MS (DDA) mode with the maximum number of precursors set to 3, the intensity cutoff threshold of 50 000 units, and active precursor exclusion after 5 MS/MS spectra. The ESI source parameters were set as follows: end plate offset 0.5 kV, capillary voltage 4 kV, nebulizing gas 2 bar, drying gas 8.0 l/min, and dry gas temperature 220°C. Measurements in MS mode were performed with an ion energy of 5.0 eV, collision energy of 7.5 eV, collision RF of 500 Vpp, the transfer time of 80 µs, pre-pulse storage of 8 µs, and low mass cutoff of 50 m/z. In MS/MS mode, ions from 50 m/z up to 1500 m/z were selected, and collision energy varied depending on precursor ion m/z and charge (for mainly observed +1 charge values were set to 25 eV for 500 m/z, 35 eV for 1000 m/z, 45 eV for 1500 m/z). An internal calibration segment was added at the beginning of each chromatographic run. Spectra were calibrated using sodium formate clusters in HPC mode with SD < 1 ppm.

The data were analyzed with Data Analysis 4.1 software. Molecular formulas corresponding to a parent and fragment ions were generated using the SmartFormula algorithm with the maximum admissible error of 5 ppm. Due to the lack of database records for newly synthesized compounds, MS/MS spectra were annotated and interpreted manually.

D. Gel Permeation Chromatography (GPC)

Number average molecular weights M_n, weight-average molecular weights M_w, mass in the maximum of signal M_p and molecular weight distributions M_w/M_n of oligomers were analyzed by GPC. The GPC setup consists of an Agilent system equipped with UV (260-700 nm), and RI detectors mixed PLGel E 3 µm, 300 x 7.5 mm column. For analysis, THF (HPLC grade, BHT stabilized, Chemsolute) was used as the mobile phase (0.5 mL/min flow rate). The standard error was calculated as the standard deviation of the mean, for three measurements of 3 samples.

E. Differential Scanning Calorimetry (DSC)

DSC curves were measured on a Mettler Toledo Differential Scanning Calorimeter. Measurements were performed under a nitrogen atmosphere (50 mL/min) in the temperature range from -50 °C to 200 °C. Three cycles of heating-cooling-heating were carried out at a heating/cooling rate of 10 K/minute. Each sample (~ 3 mg) was loaded in an aluminum pan. Indium was used as a reference substance. T_g values were determined from the inflection point of the second heating endotherm by the spreadsheet calculator. [1,2] T_m were determined as a minimum of the first endothermic signal. Samples before DSC measurement were heated in an oil bath at 100 °C, under a vacuum for about 5-10 minutes to remove solvent traces.

F. Fourier Transform Infrared Spectroscopy (FTIR)

The chemical structure of the samples was examined by the Fourier Transform Infrared Spectroscopy (FTIR) with the Attenuated Total Reflectance (ATR) diamond attachment using the Bruker FTIR Tensor 27 EQ apparatus. The spectra have been registered in the range of 350–4000 cm^{-1} (32 scans) with 4 cm^{-1} resolution.

G. Thermal Gravimetric Analysis (TGA)

Thermogravimetric analyses were performed using Mettler Toledo TGA 2 - Thermogravimetric Analyzer with a large furnace (LF). The measurements (5 mg of each sample) were carried out from 25 to 500 °C with a 10 K/min heating rate under and inert atmosphere (N_2 flow 30 mL/min).

H. Thermal Gravimetric Analysis - Fourier Transform Infrared Spectroscopy (TGA-FTIR)

Thermal degradations studies were performed using a thermogravimetric analyzer (STA449 F1 Jupiter, Netzsch) coupled with an FTIR spectrometer (Tensor 27 EQ spectrophotometer, Bruker). The analyses were performed during increasing temperature from 30 to 500 °C with a 10 K/min heating rate in a nitrogen atmosphere (flow 50 mL/min). TG and FTIR simultaneous thermal analysis of gases formed during the decomposition process of selected samples was performed for 2 mg of samples placed in alumina crucibles. The FTIR spectra were recorded in the range of 650–4000 cm^{-1} (16 scans) with 2 cm^{-1} resolution.

III. Results and Discussion

A. Synthesis of oligourethanes

Table S1. Amount of used reagents for synthesis OU1-OU10.

OLIGOMER	ACTIVATION						COUPLING	EXTRACTION			
	Bz-OH		DSC [eq]	PYR [eq]	ACN [ml]	Anisole [µL]	Amino-alcohol [eq]				
	eq	g						I	II	III	IV
Bz-AAAA	1	0.2	1.2	3	6	5	1.2	EtAc	EtAc	EtAc	EtAc
Bz-BAAA	1	0.2	1.2	3	6	5	1.2	EtAc	EtAc	EtAc	EtAc
Bz-ABAA	1	0.2	1.2	3	6	5	1.2	EtAc	EtAc	EtAc	EtAc
Bz-BBAA	1	0.2	1.2	3	6	5	1.2	EtAc	EtAc	EtAc	DCM
Bz-BBBA	1	0.2	1.2	3	6	5	1.2	EtAc	EtAc	EtAc	DCM
Bz-BBBB	1	0.2	1.2	3	6	5	1.2	EtAc	EtAc	EtAc	DCM
Bz-ABBA	1	0.2	1.2	3	6	5	1.2	EtAc	EtAc	EtAc	DCM
Bz-BABA	1	0.2	1.2	3	6	5	1.2	EtAc	EtAc	EtAc	EtAc
Bz-ACAA	1	0.2	1.2	3	6	5	1.2	EtAc	EtAc	DCM	DCM
Bz-CBCC	1	0.2	1.2	3	6	5	1.2	EtAc	EtAc	EtAc	EtAc

Table S2. Stepwise yields of oligomer syntheses OU1-OU10.

OU1 Bz-AAAA	
Reaction step	**Yield after each step [%]**
I coupling	84.8
II coupling	98.1
III coupling	90.0
IV coupling	85.6

OU2 Bz-BAAA	
Reaction step	**Yield after each step [%]**
I coupling	94.0
II coupling	94.6
III coupling	82.0
IV coupling	71.5

OU3 Bz-ABAA	
Reaction step	**Yield after each step [%]**
I coupling	85.1
II coupling	92.0
III coupling	84.5
IV coupling	85.6

OU4 Bz-BBAA	
Reaction step	**Yield after each step [%]**
I coupling	94.0
II coupling	97.6
III coupling	76.5
IV coupling	60.0

OU5 Bz-BBBA	
Reaction step	**Yield after each step [%]**
I coupling	94.0
II coupling	97.6
III coupling	71.0
IV coupling	67.2

OU6 Bz-BBBB	
Reaction step	**Yield after each step [%]**
I coupling	98.8
II coupling	99.1
III coupling	75.4
IV coupling	63.7

O7 Bz-ABBA	
Reaction step	**Yield after each step [%]**
I coupling	74.4
II coupling	87.6
III coupling	83.1
IV coupling	77.8

O8 Bz-BABA	
Reaction step	**Yield after each step [%]**
I coupling	94.0
II coupling	94.6
III coupling	97.7
IV coupling	70.0

OU9 Bz-ACAA	
Reaction step	**Yield after each step [%]**
I coupling	84.8
II coupling	98.1
III coupling	90.0
IV coupling	85.6

OU10 Bz-CBCC	
Reaction step	**Yield after each step [%]**
I coupling	84.8
II coupling	98.1
III coupling	90.0
IV coupling	85.6

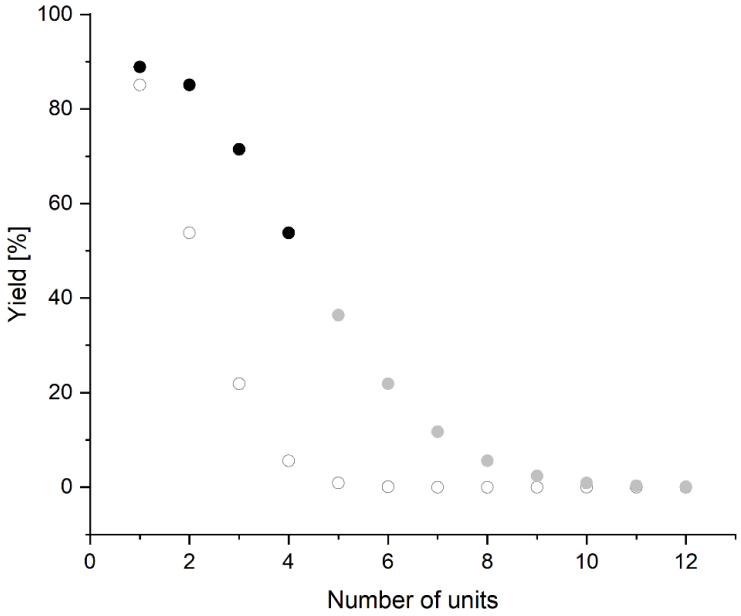

Chart S1. Comparison of overall yields between classical solution synthesis and optimized one-pot coupling protocol. Average overall yields of solution synthesis (●) and simulated yields with the increase of oligomer length (●) (calculated based on the average decrease of yield). Simulated yields for synthesis with extraction after each activation and coupling step (○) calculated based on the average decrease of yield. The method is relevant for eight couplings as we predicted based on average yields, that will lead to octamer. To reach for longer oligomers we should combine our protocol with an iterative exponential growth approach (DP=2, 4, 8,16 …), that after eight steps gives polymer of DP=256.

Table S3. Characterization of OU1-OU10.

	Sequence[a]	Molar mass[b]	m/z[c]	Purity [%][d]	Yield [%][e]	Scale [g][f]
OU1	Bz-AAAA	512.55	513.26	95.7	55.7	0.385
OU2	Bz-BAAA	512.55	513.26	94.0	55.7	0.523
OU3	Bz-ABAA	512.55	513.26	94.0	74.6	0.707
OU4	Bz-BBAA	512.55	513.26	94.0	41.0	0.382
OU5	Bz-BBBA	512.55	513.26	92.0	43.7	0.334
OU6	Bz-BBBB	512.55	513.26	97.0	47.9	0,240
OU7	Bz-ABBA	512.55	513.26	94.3	42.5	0.379
OU8	Bz-BABA	512.55	513.26	96.0	56.5	0.525
OU9	Bz-ACAA	574.62	575.27	97.0	42.5	0.373
OU10	Bz-CBCC	698.76	699.30	47.3 (before flash chromatography) 100 (after flash chromatography)	63.4	0.812

[a]Abbreviations: A - 3-amino-1-propanol, B - (S)-2-amino-1-propanol, C - 3-(aminomethyl)benzyl alcohol, Bz – benzyl alcohol; [b]calculated molar mass, [c]mass determined from LC-MS;[d]calculated from HPLC; [e]overall yield; [f]mass of the obtained product.

B. ^{1}H Nuclear Magnetic Resonance Spectroscopy (^{1}H NMR)

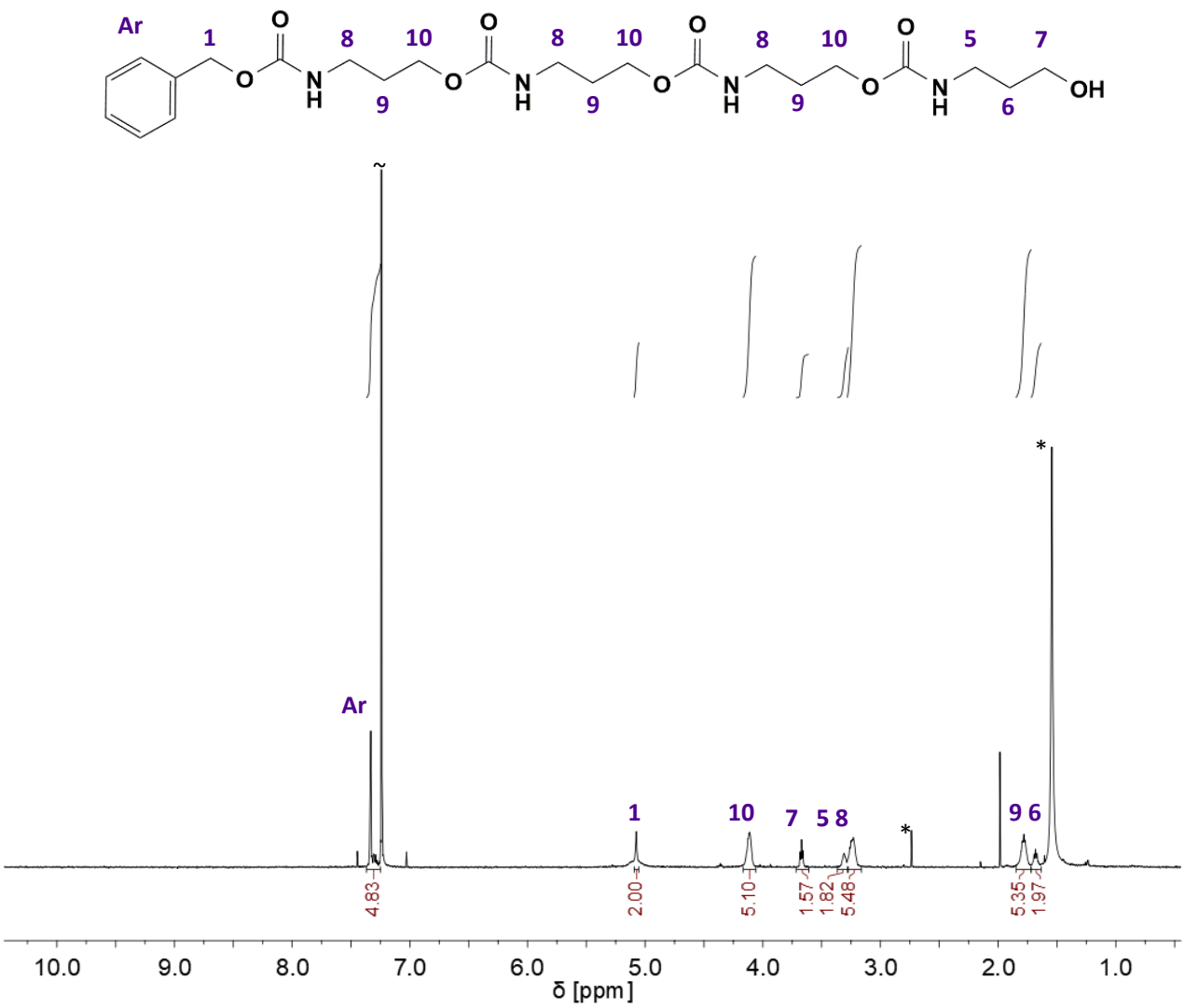

Figure S2. ^{1}H NMR spectra of **OU1** Bz-AAAA recorded in $CDCl_3$.

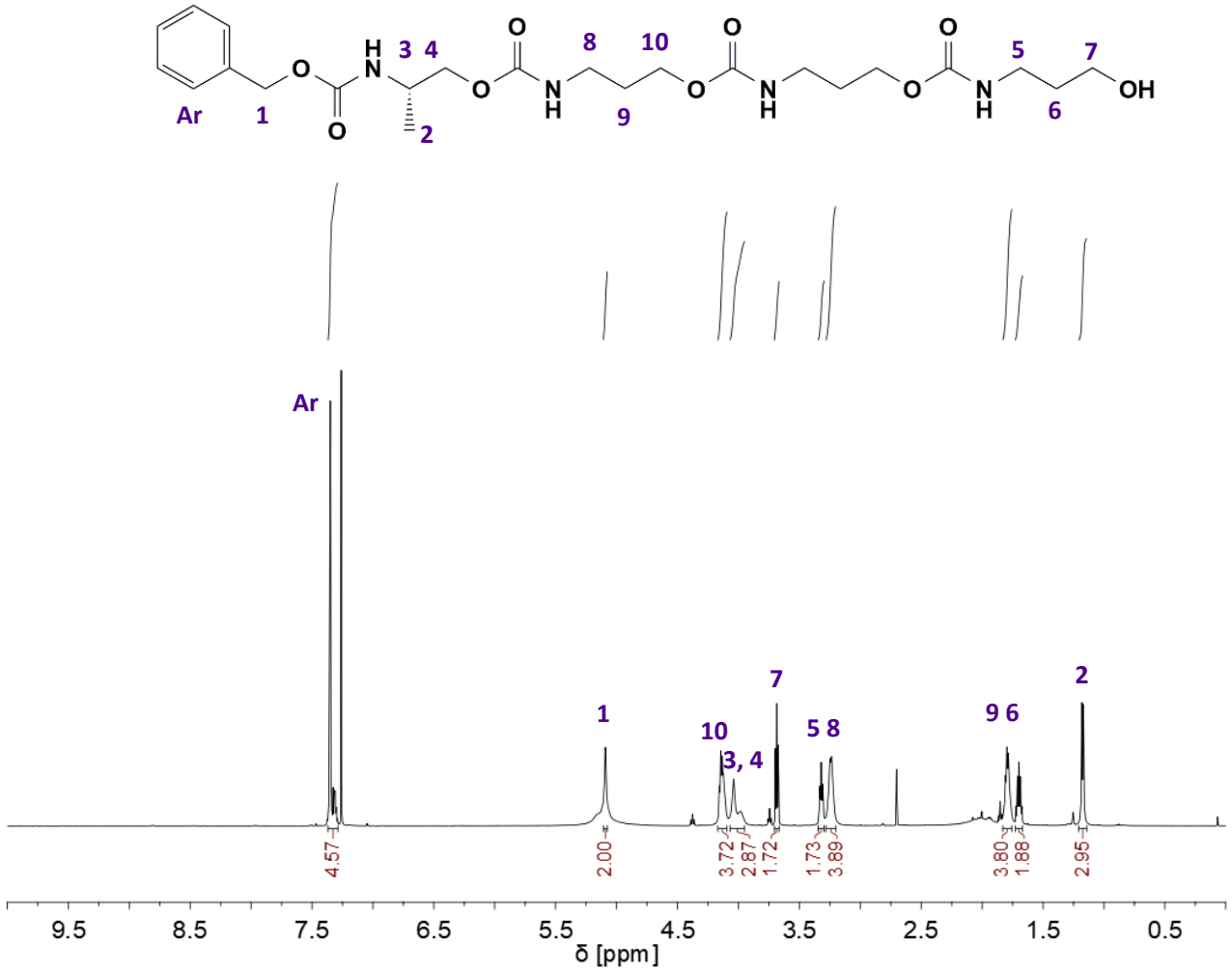

Figure S3. ^{1}H NMR spectra of **OU2** Bz-BAAA recorded in $CDCl_3$.

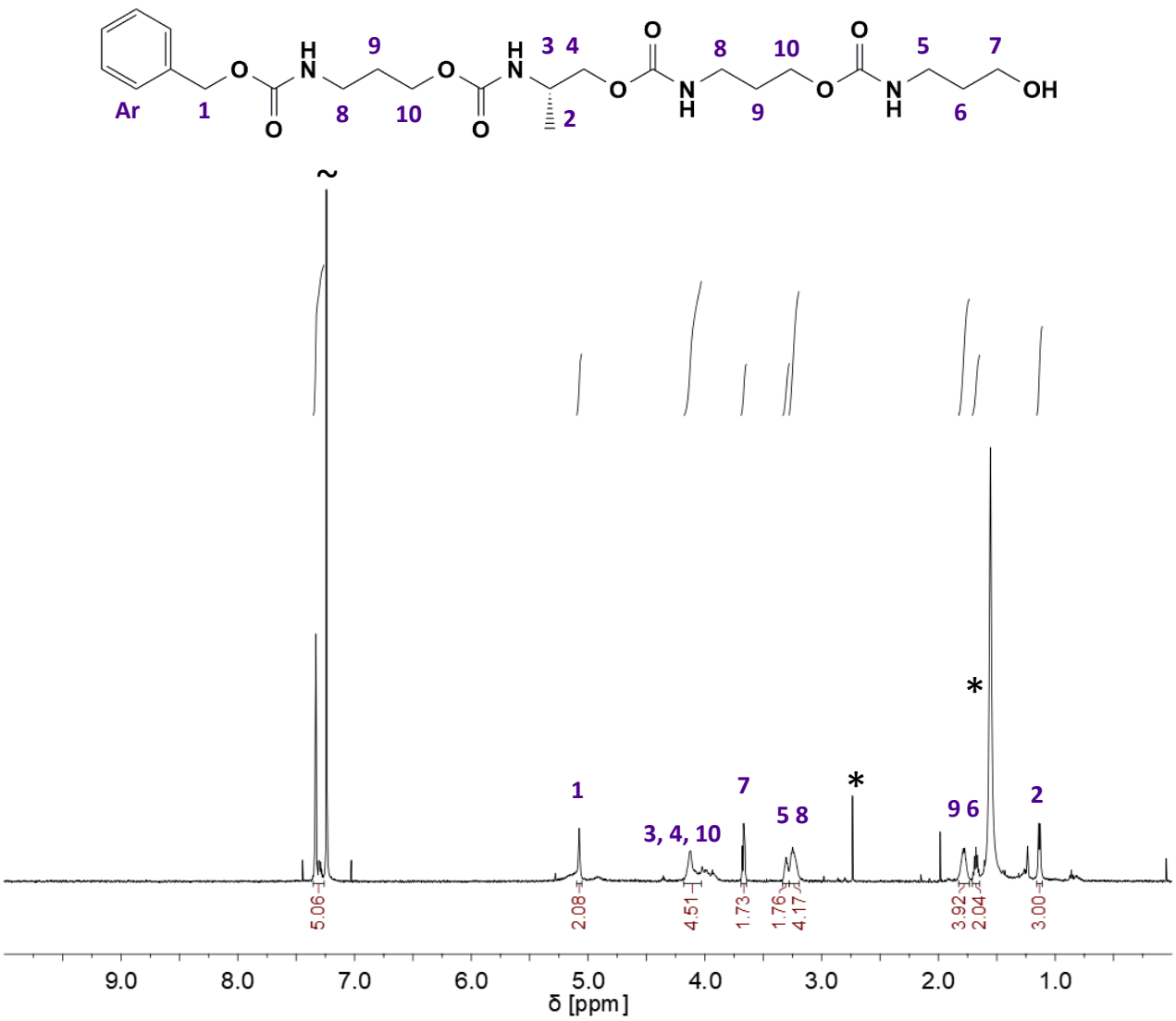

Figure S4. ^{1}H NMR spectra of **OU3** Bz-ABAA recorded in $CDCl_3$.

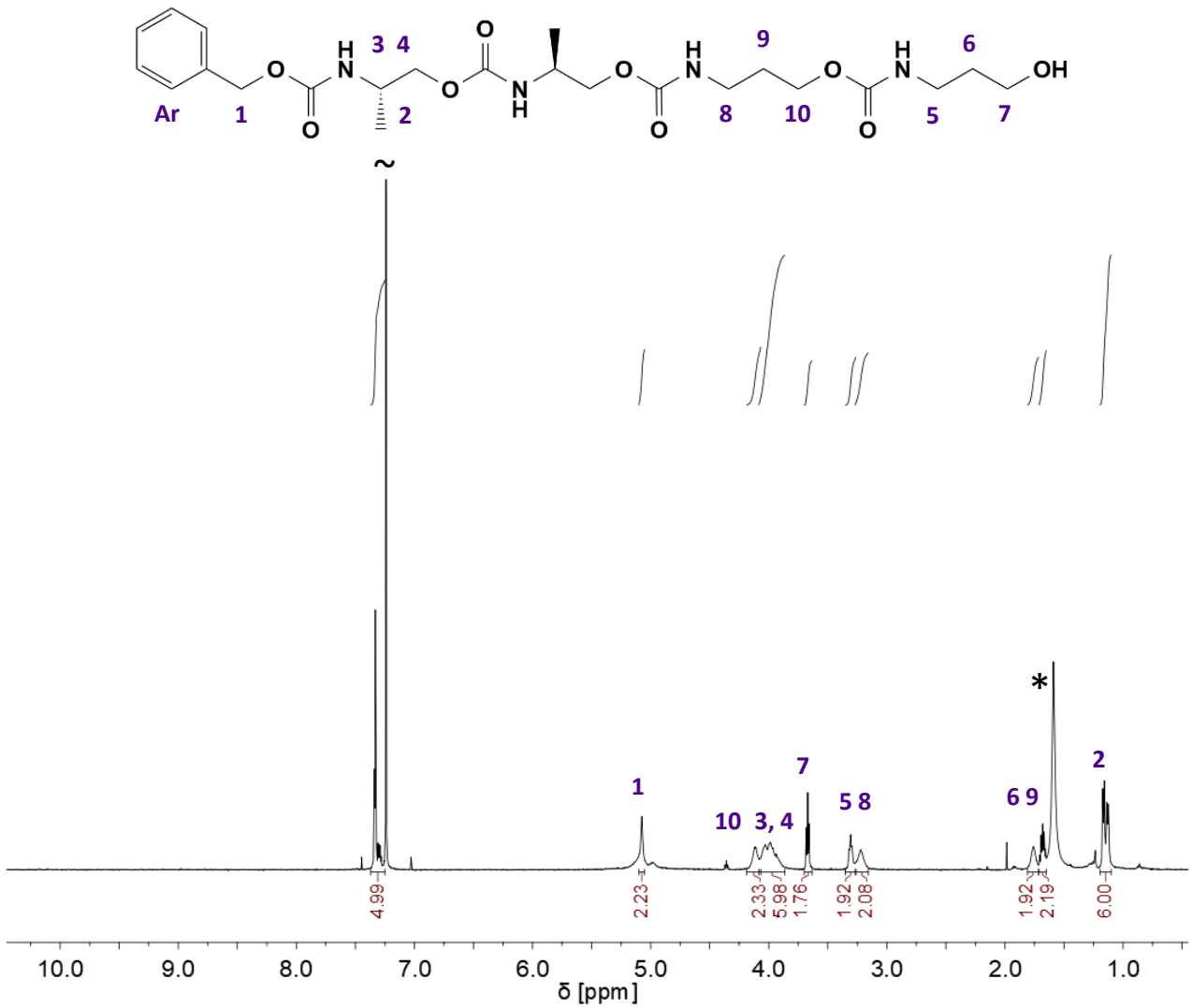

Figure S5. ^{1}H NMR spectra of **OU4** Bz-BBAA recorded in $CDCl_3$.

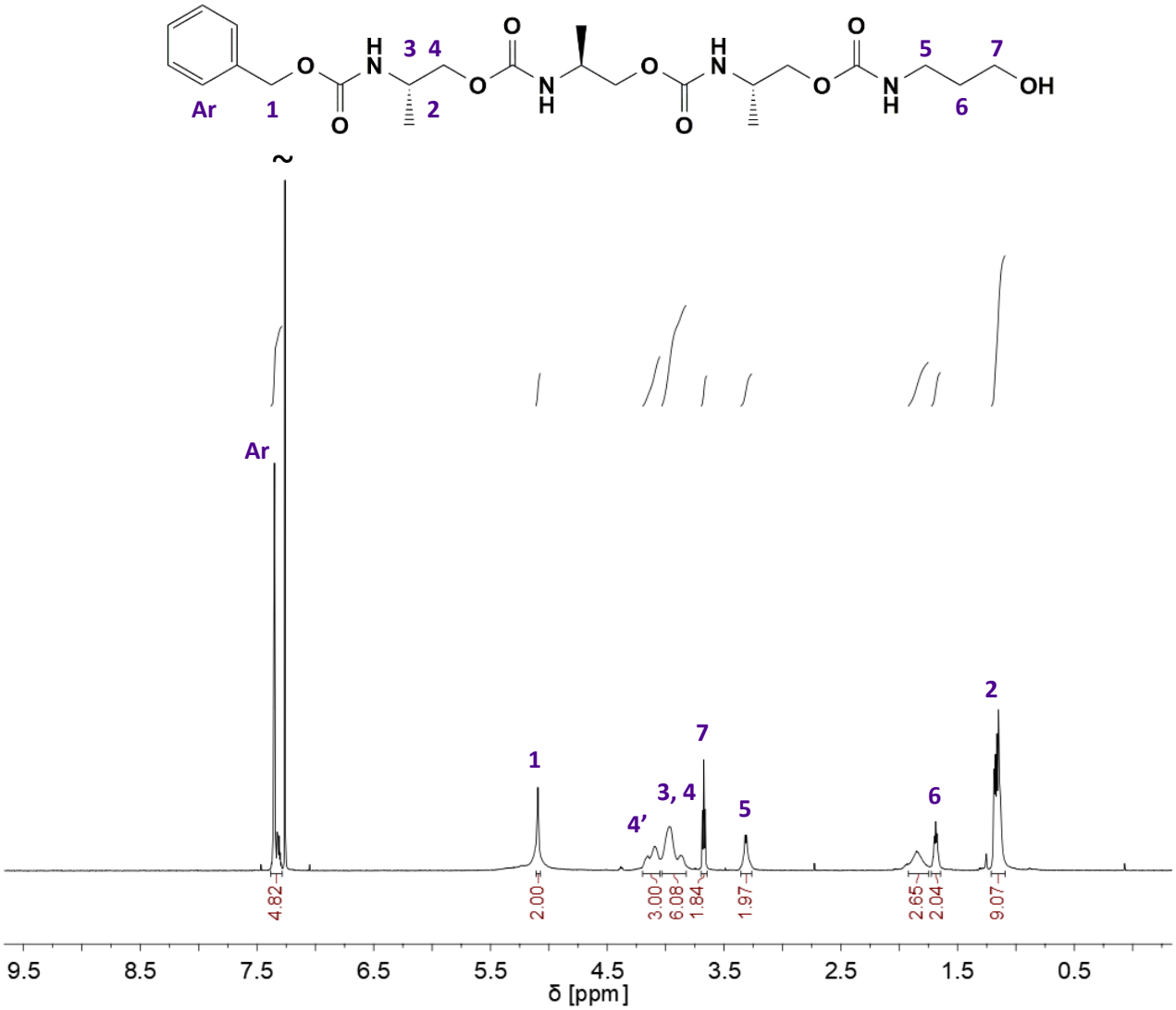

Figure S6. ^{1}H NMR spectra of **OU5** Bz-BBBA recorded in $CDCl_3$.

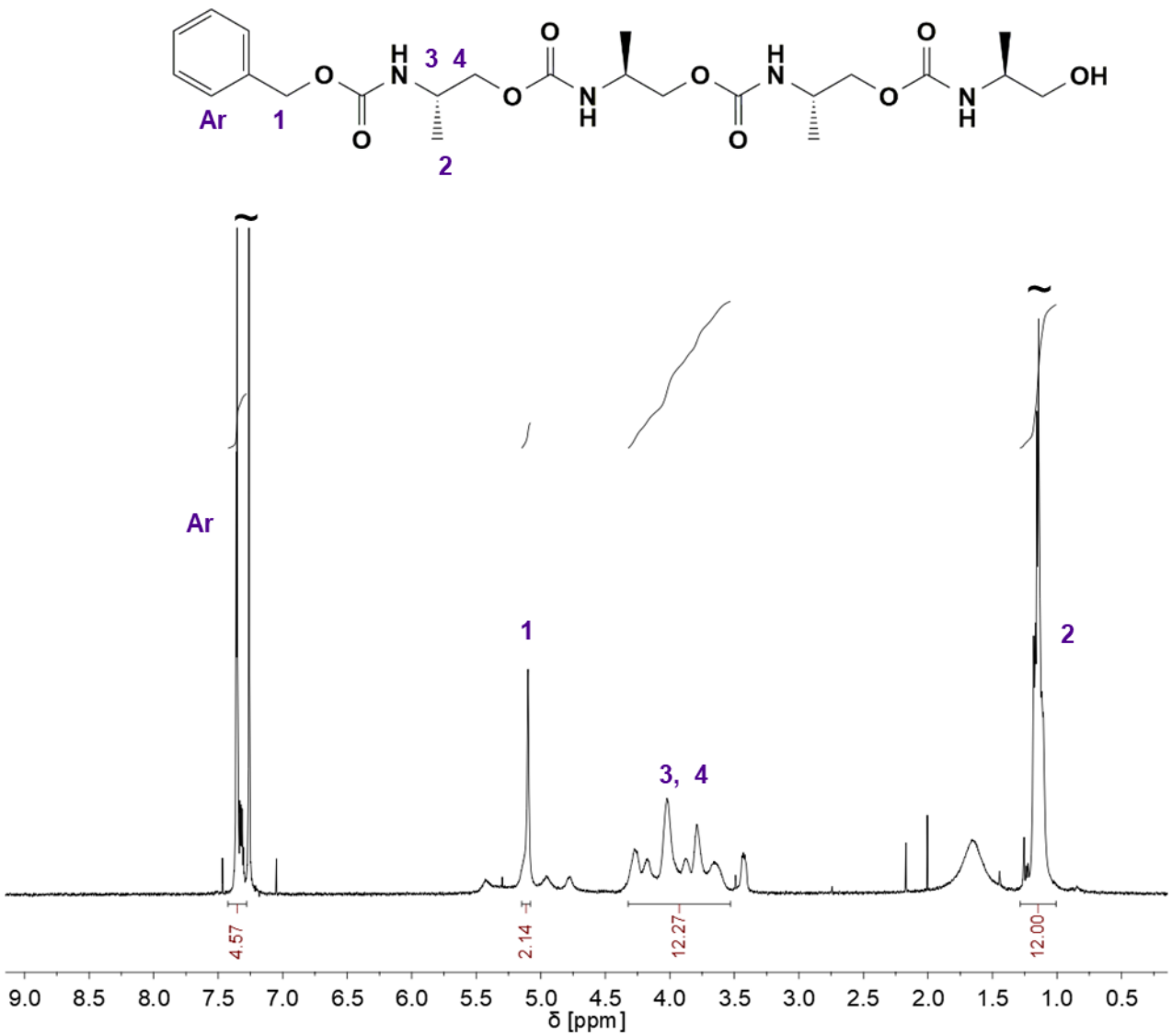

Figure S7. ^{1}H NMR spectra of **OU6** Bz-BBBB recorded in $CDCl_3$.

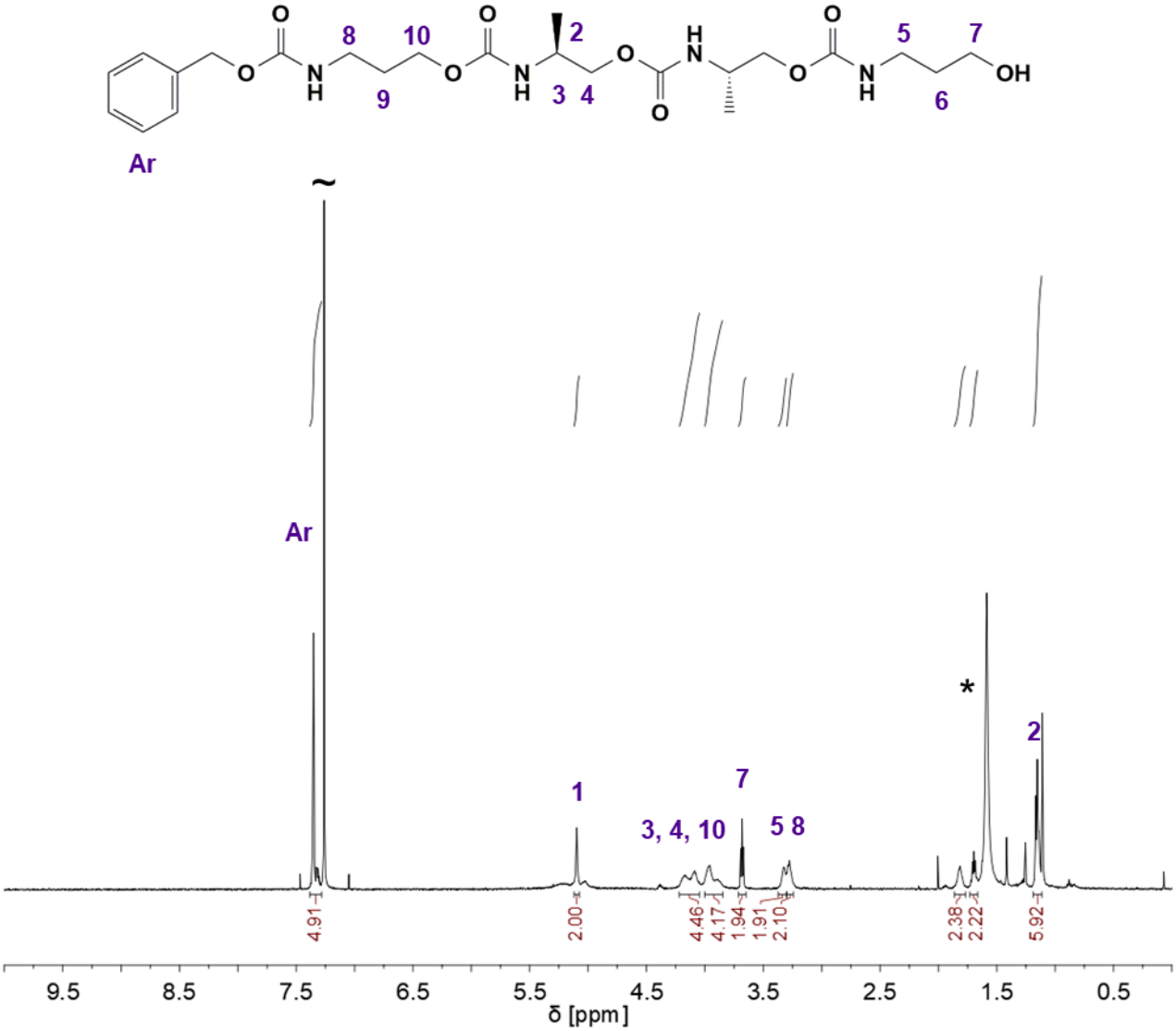

Figure S8. ^{1}H NMR spectra of **OU7** Bz-ABBA recorded in $CDCl_3$.

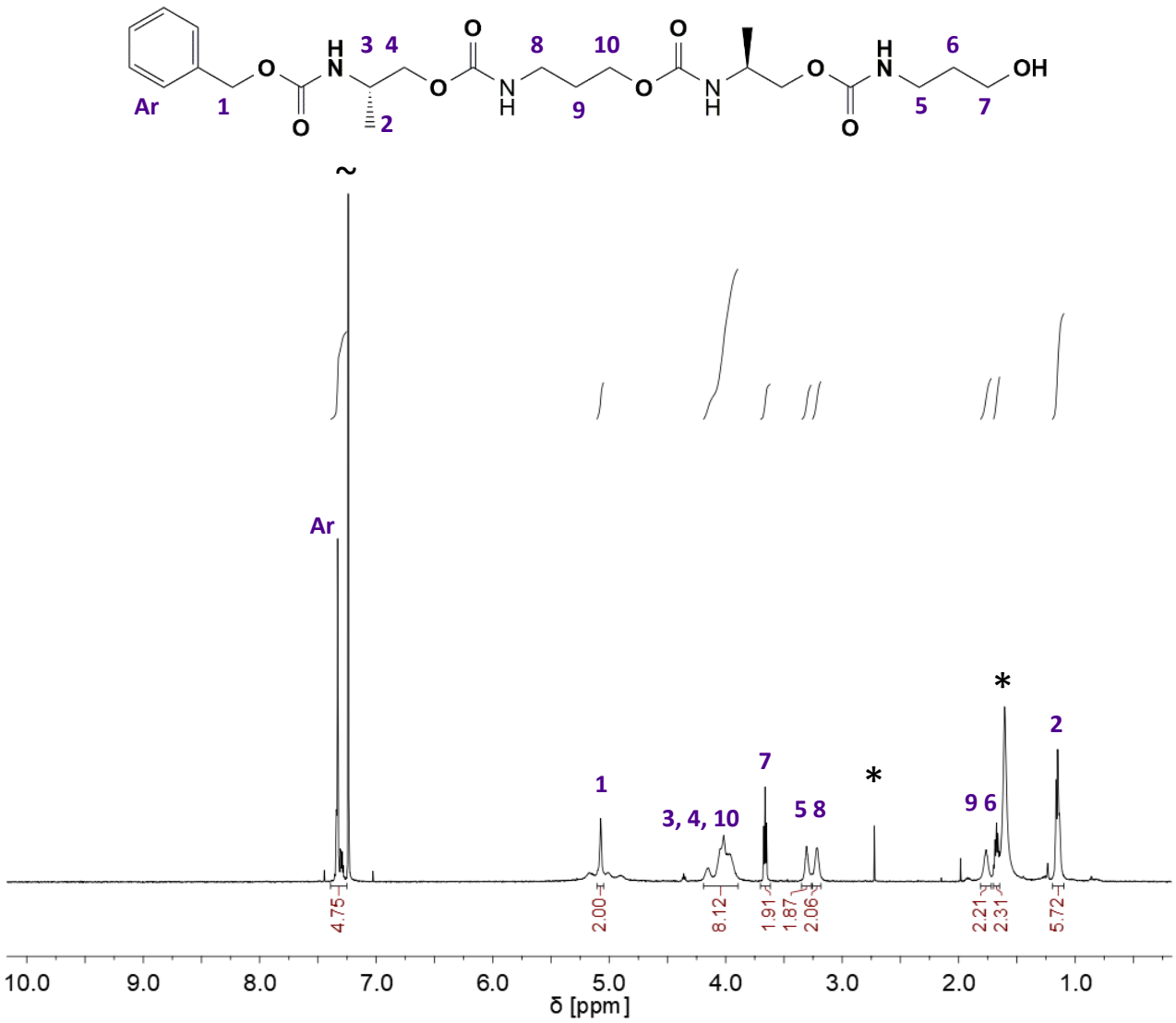

Figure S9. ^{1}H NMR spectra of **OU8** Bz-BABA recorded in $CDCl_3$.

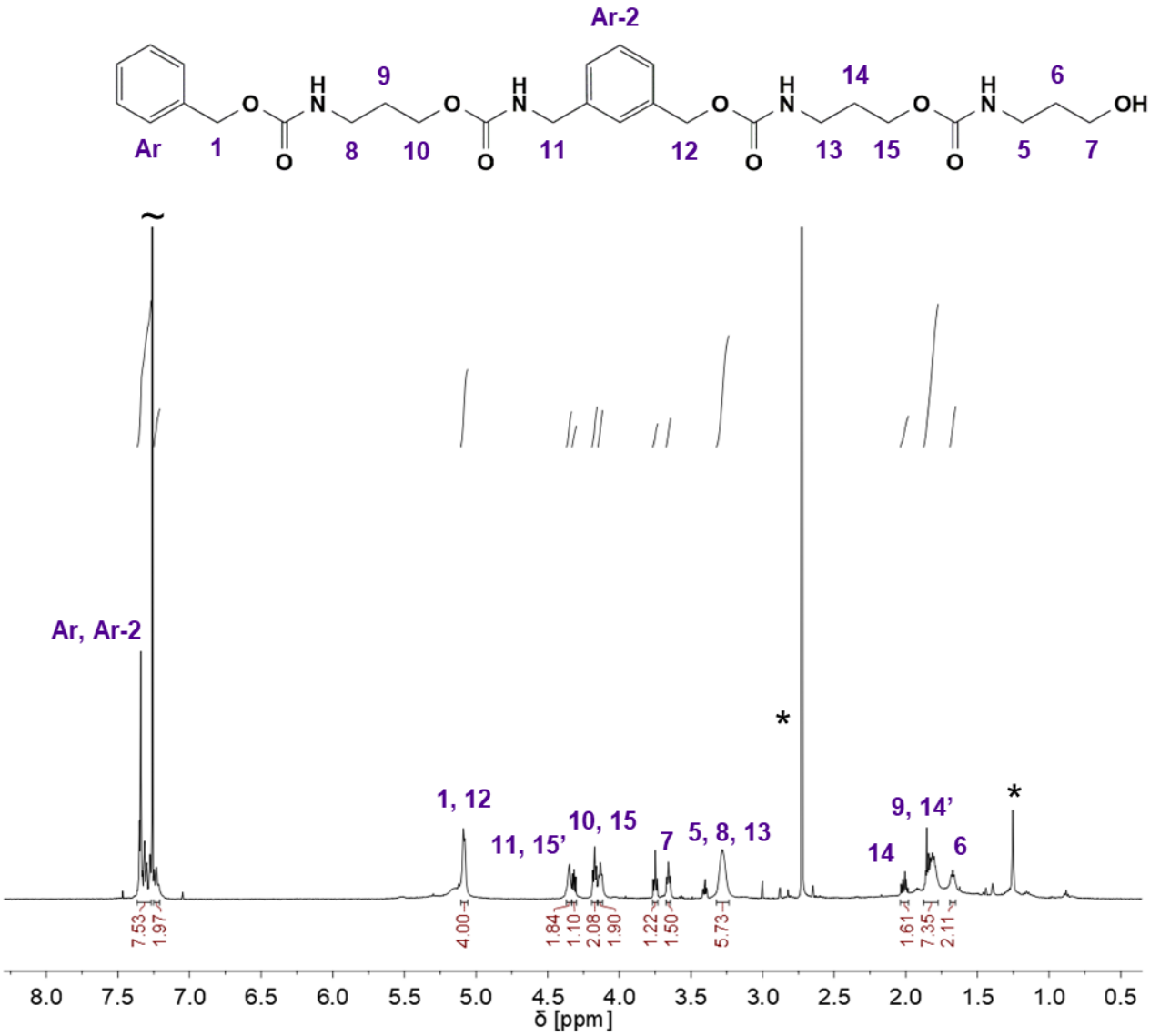

Figure S10. ^{1}H NMR spectra of **OU9** Bz-ACAA recorded in $CDCl_3$.

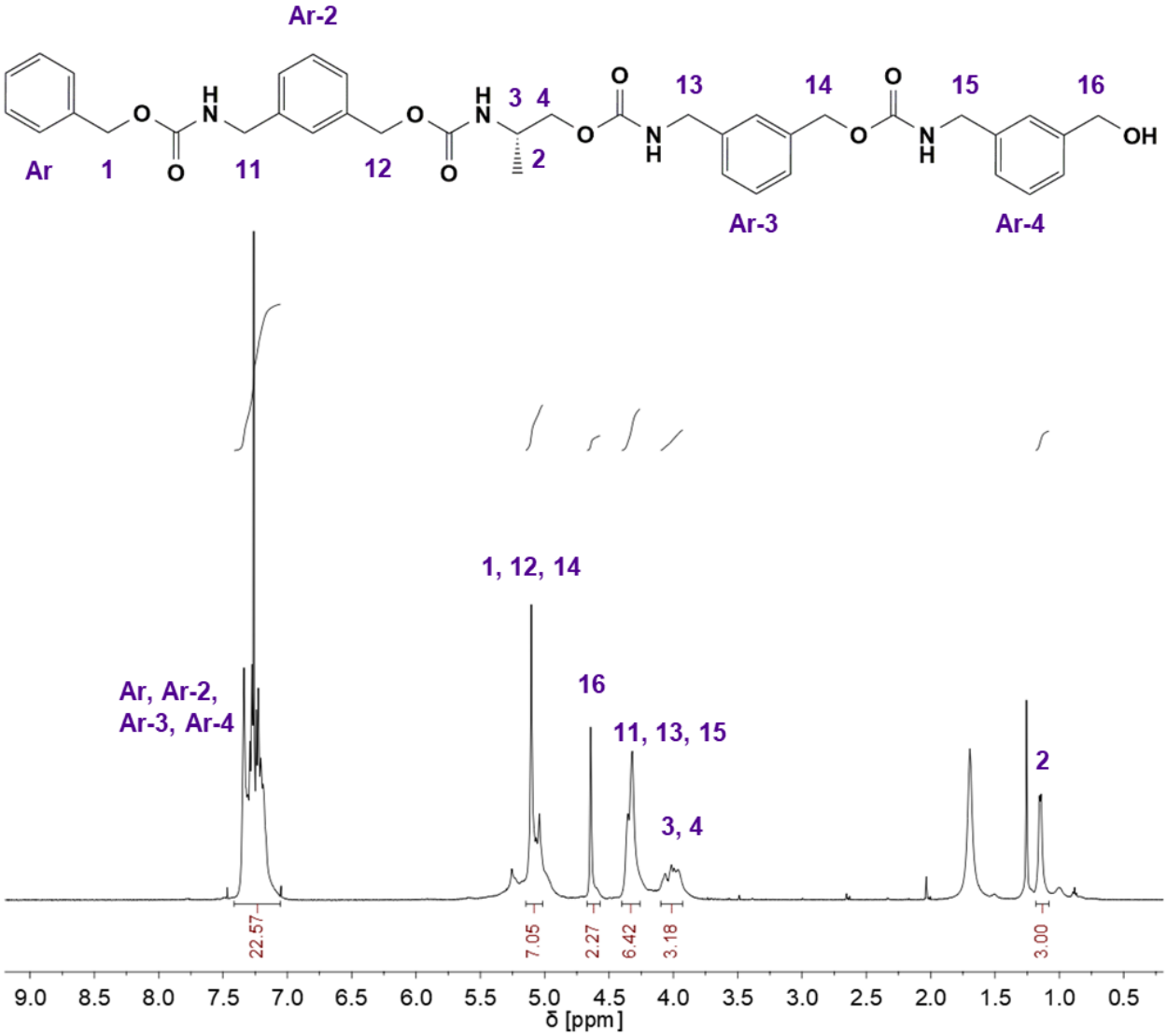

Figure S11. ^{1}H NMR spectra of **OU10** Bz-CBCC recorded in $CDCl_3$.

C. Gel Permeation Chromatography (GPC)

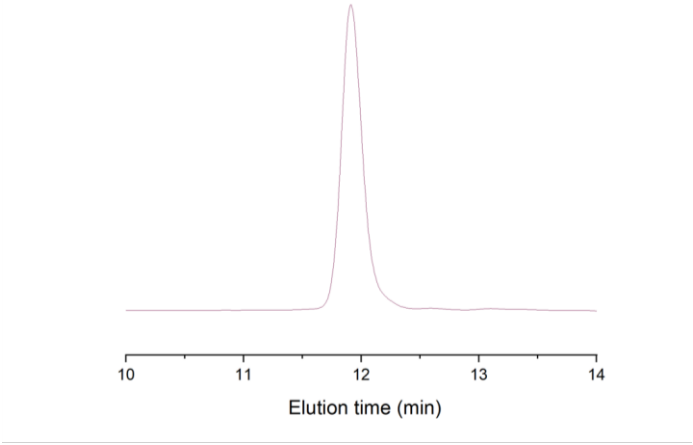

Figure S12. GPC of **OU1** Bz-AAAA recorded in THF.

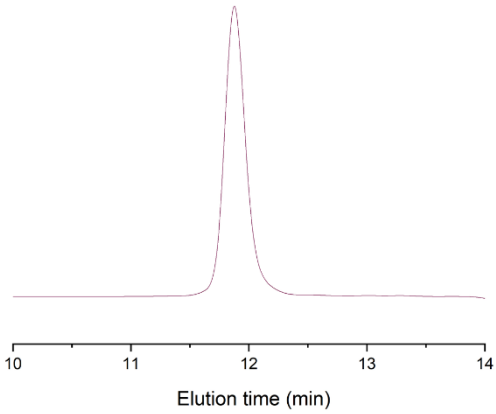

Figure S13. GPC of **OU2** Bz-BAAA recorded in THF.

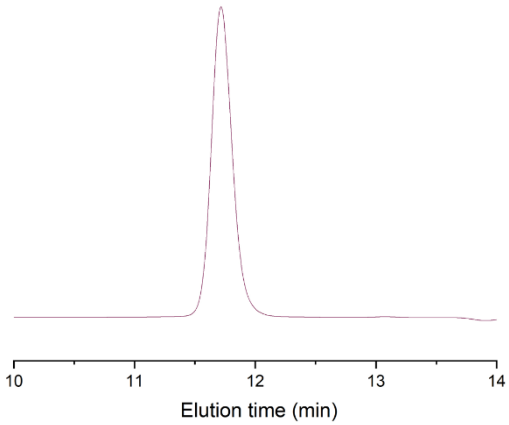

Figure S14. GPC of **OU3** Bz-ABAA recorded in THF.

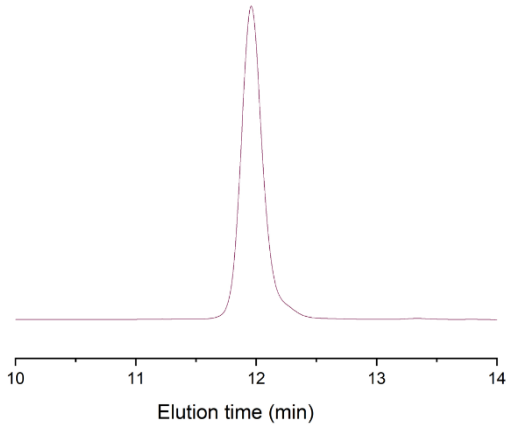

Figure S15. GPC of **OU4** Bz-BBAA recorded in THF.

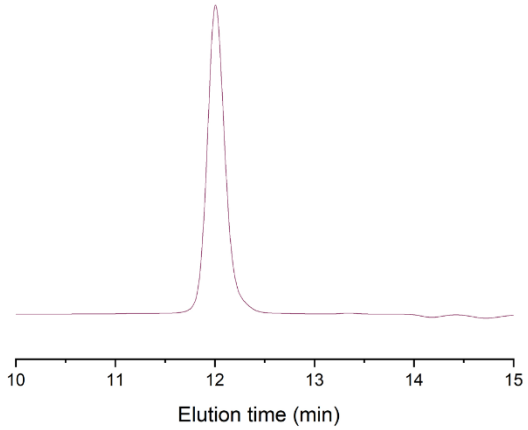

Figure S16. GPC of **OU5** Bz-BBBA recorded in THF.

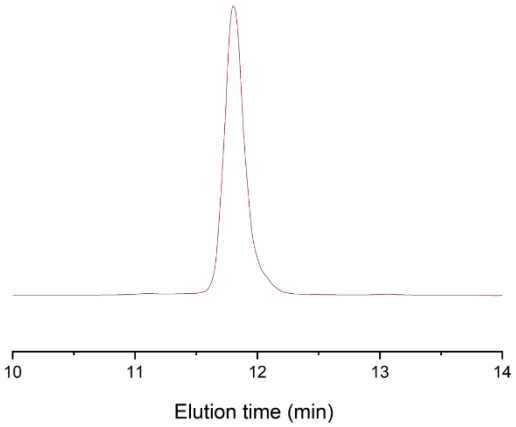

Figure S17. GPC of **OU6** Bz-BBBB recorded in THF.

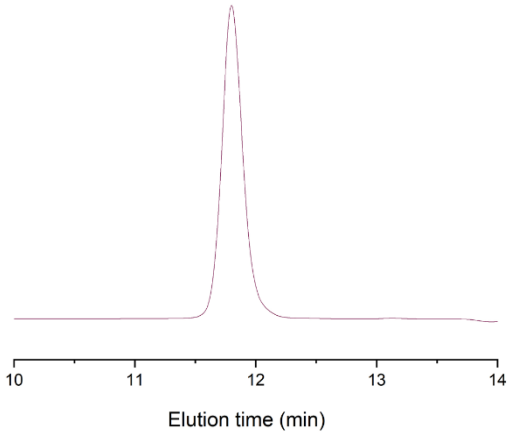

Figure S18. GPC of **OU7** Bz-ABBA recorded in THF.

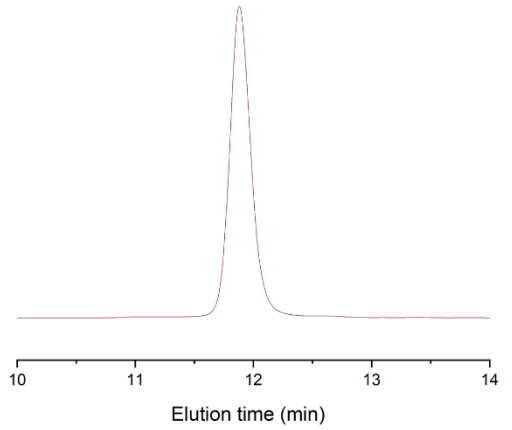

Figure S19. GPC of **OU8** Bz-BABA recorded in THF.

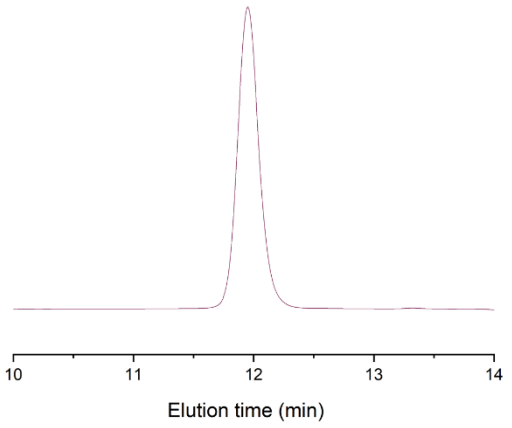

Figure S20. GPC of **OU9** Bz-ACAA recorded in THF.

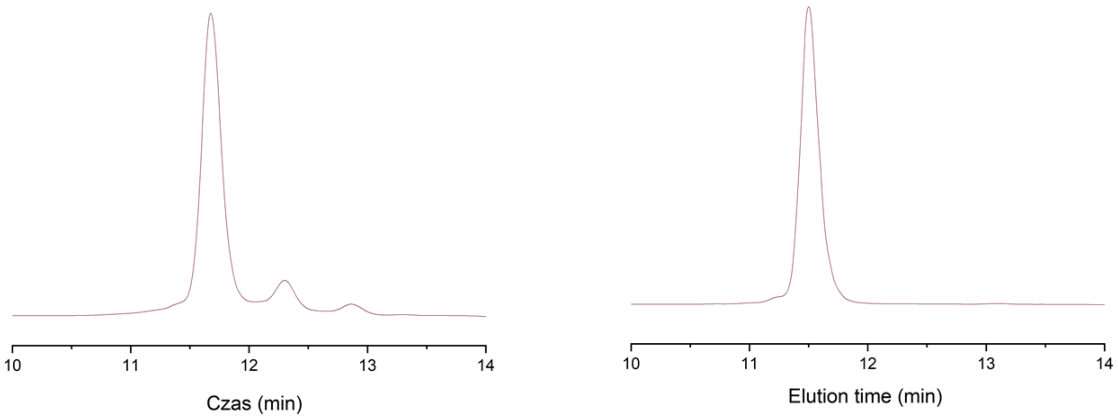

Figure S21. GPC of **OU10** Bz-CBCC recorded in THF, before (left) and after (right) flash chromatography.

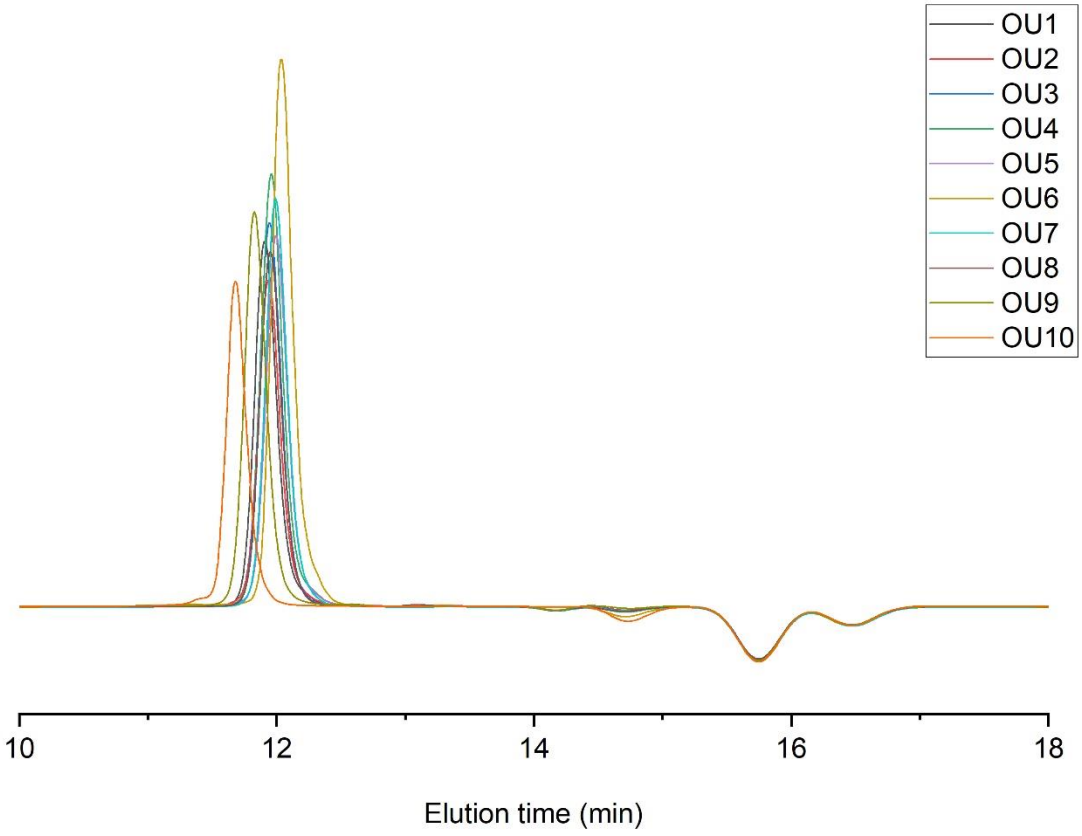

Figure S22. GPC of all oligomers OU1-OU10 recorded in THF, all chromatograms were normalized according to signal at 15.8 min to determine M_p values.

D. Liquid chromatography–mass spectrometry (LC-MS)

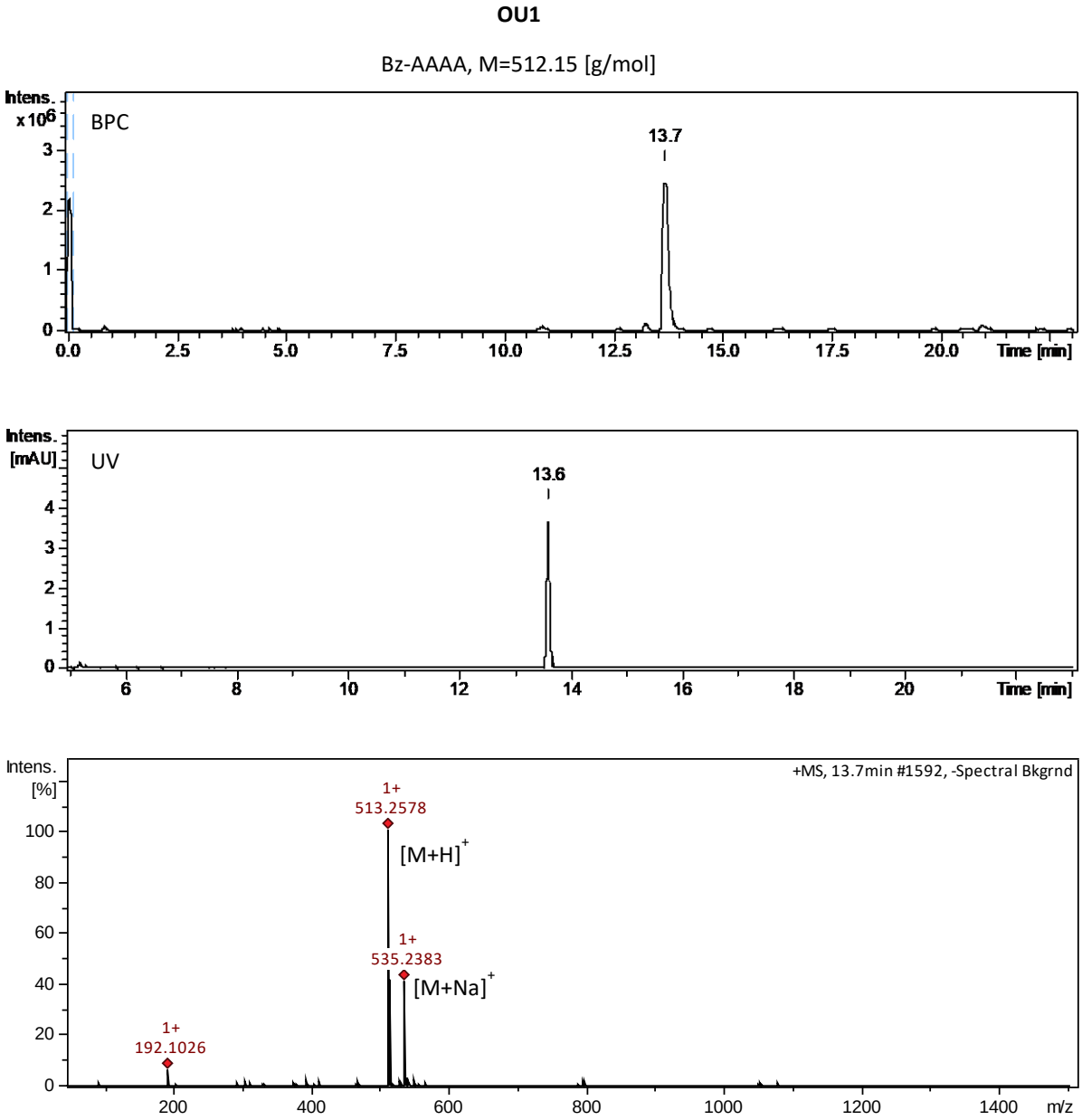

Figure S23. LC-MS characterization of crude Bz-AAAA. The main signal corresponds to the product **OU1**. It appears in the spectrum in the form of two adducts: $[M+H]^+$ (m/z=513.2578) and $[M+Na]^+$ (m/z=535.2383).

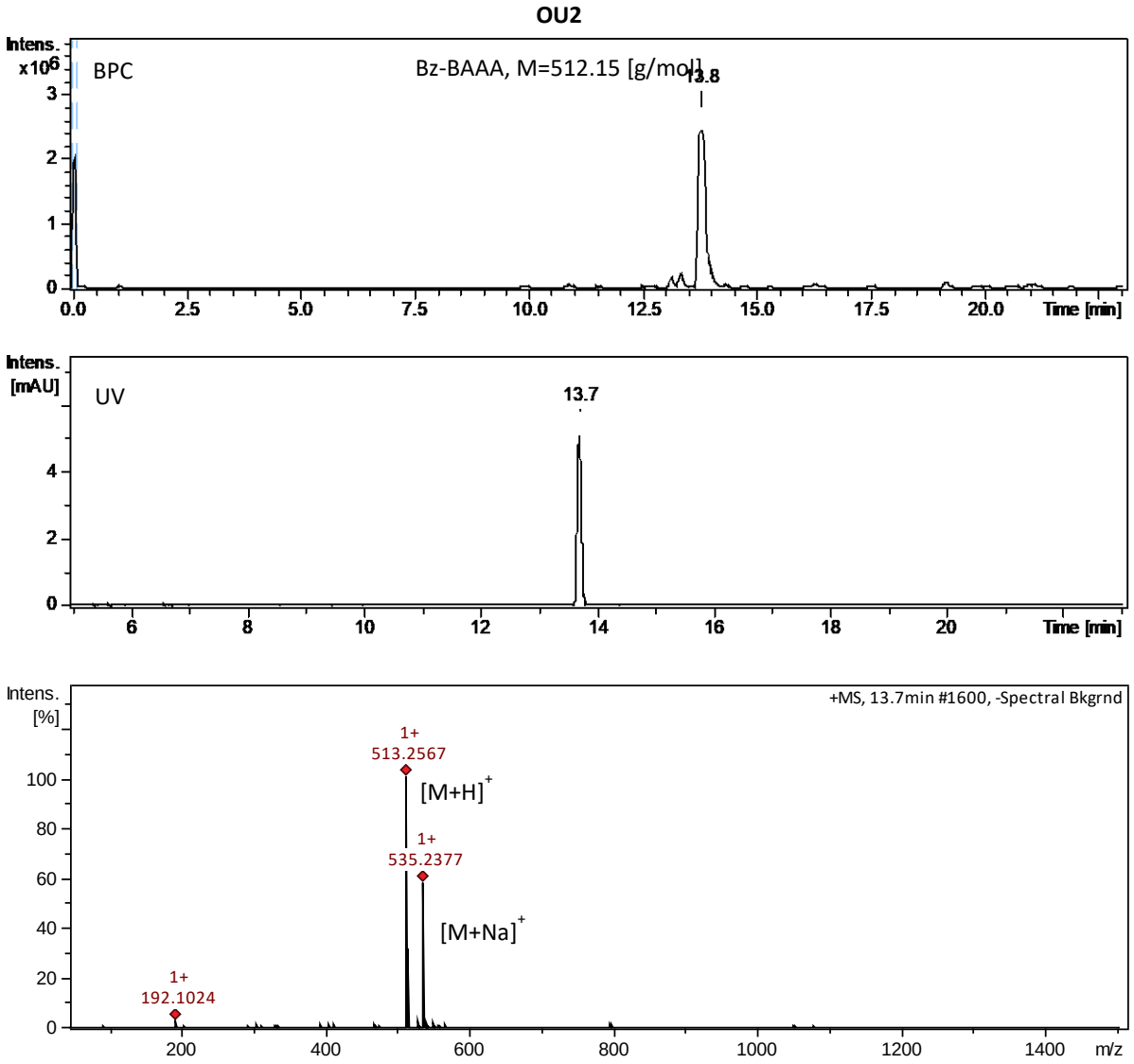

Figure S24. LC-MS characterization of crude Bz-BAAA. The main signal corresponds to the product **OU2**. It appears in the spectrum in the form of two adducts: $[M+H]^+$ (m/z=513.2567) and $[M+Na]^+$ (m/z=535.2377).

OU3

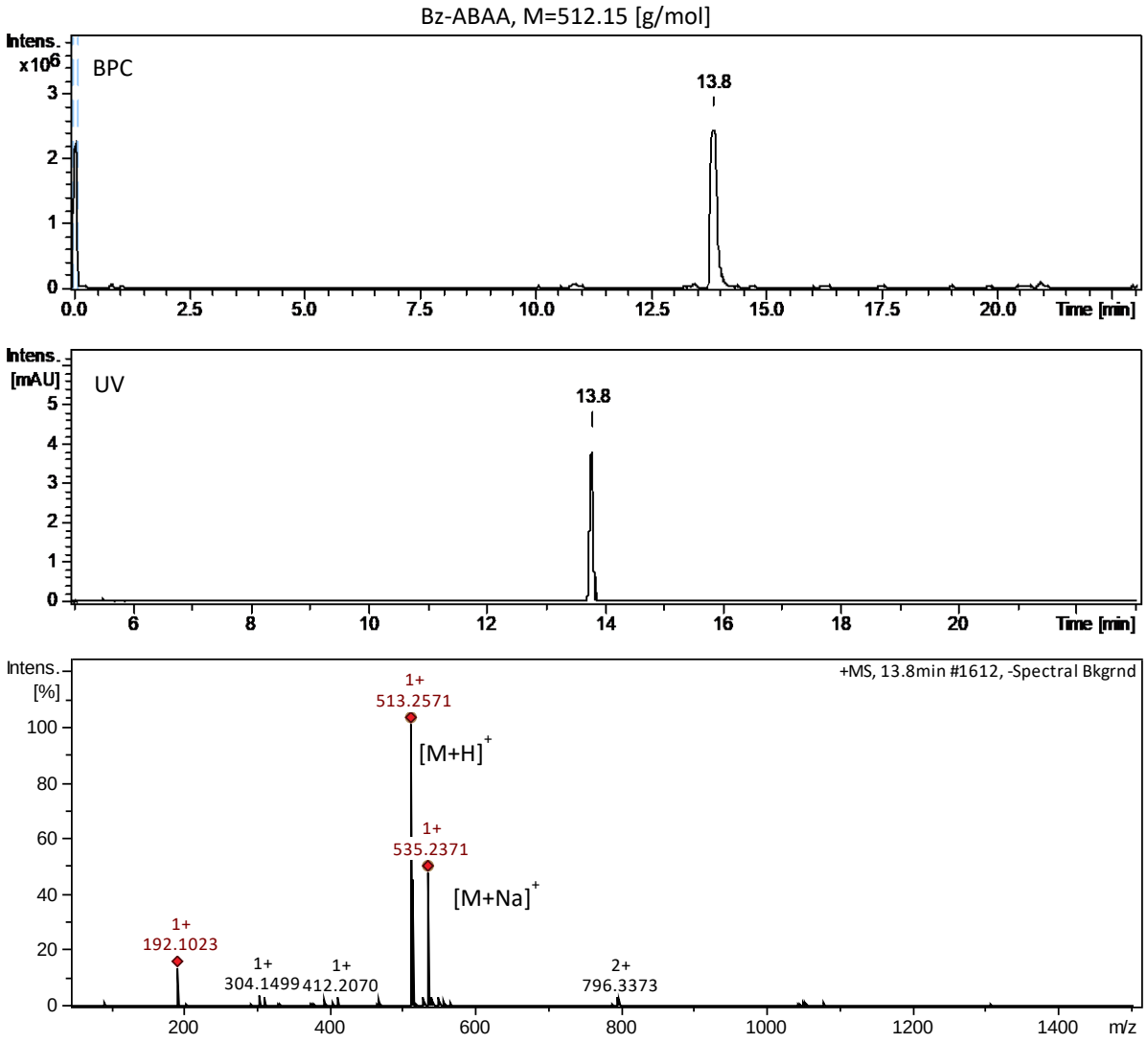

Figure S25. LC-MS characterization of crude Bz-ABAA. The main signal corresponds to the product **OU3**. It appears in the spectrum in the form of two adducts: $[M+H]^+$ (m/z=513.2571) and $[M+Na]^+$ (m/z=535.2371).

OU4

Bz-BBAA, M=512.15 [g/mol]

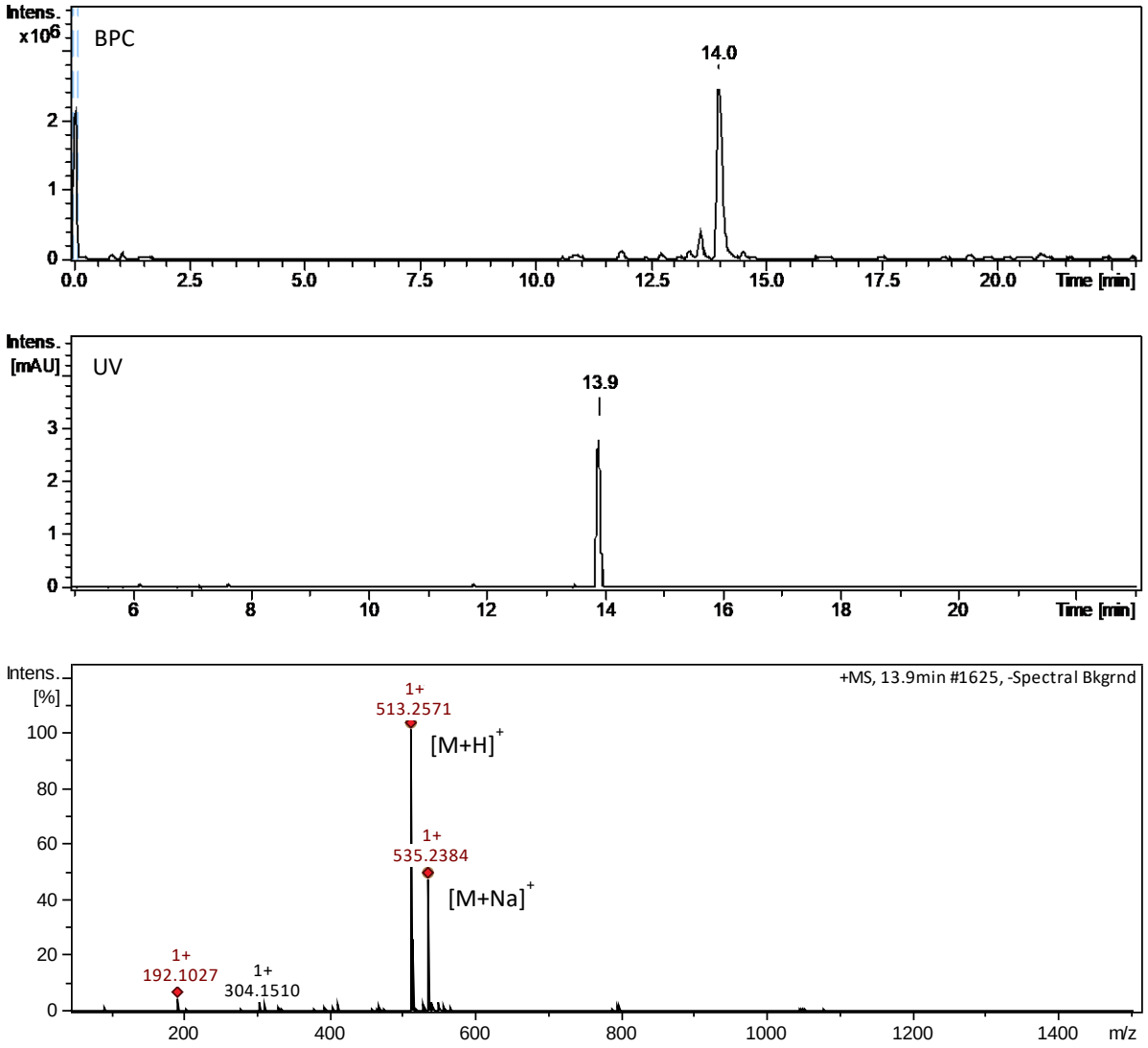

Figure S26. LC-MS characterization of crude Bz-BBAA. The main signal corresponds to the product **OU4**. It appears in the spectrum in the form of two adducts: $[M+H]^+$ (m/z=513.2571) and $[M+Na]^+$ (m/z=535.2384).

OU5

Bz-BBBA, M=512.15 [g/mol]

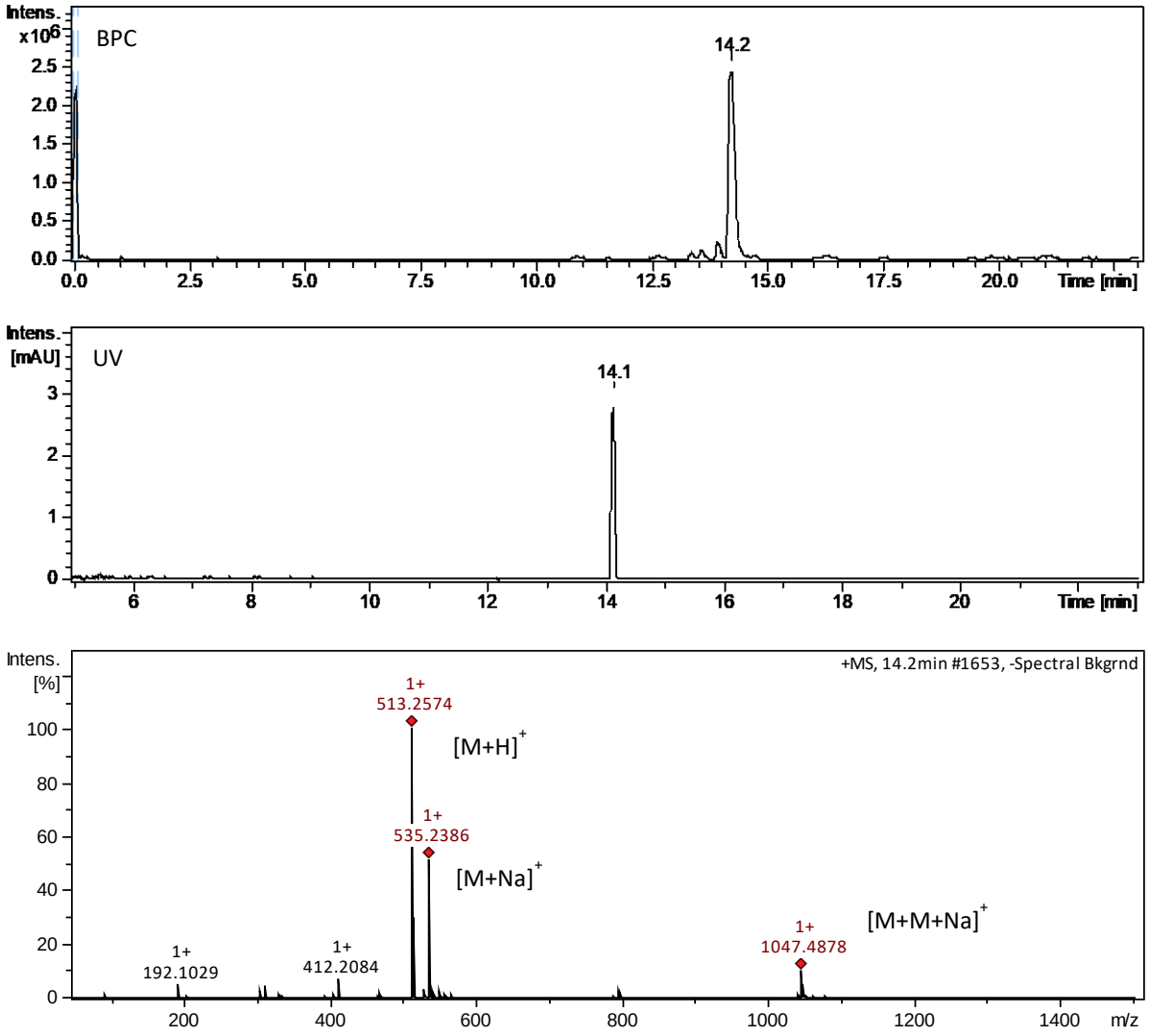

Figure S27. LC-MS characterization of crude Bz-BBBA. The main signal corresponds to the product **OU5**. It appears in the spectrum in the form of three adducts: $[M+H]^+$ (m/z=513.2574), $[M+Na]^+$ (m/z=535.2386) and $[M+M+Na]^+$ (m/z=1047.4878).

OU6

Bz-BBBB, M=512.15 [g/mol]

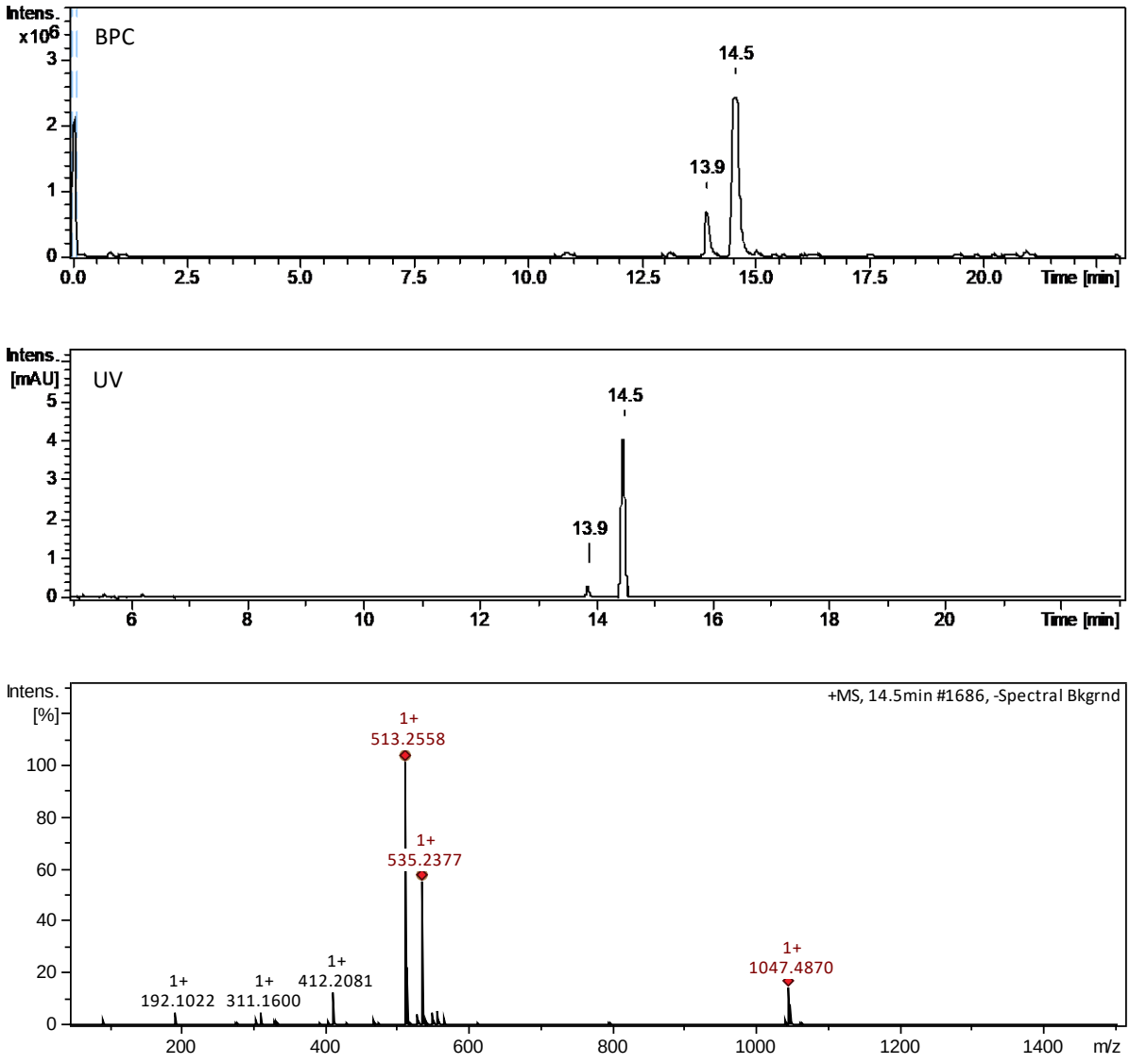

Figure S28. LC-MS characterization of crude Bz-BBBB. The main signal corresponds to the product **OU6**. It appears in the spectrum in the form of three adducts: $[M+H]^+$ (m/z=513.2558), $[M+Na]^+$ (m/z=535.2377) and $[M+M+Na]^+$ (m/z=1047.4870).

OU7

Bz-ABBA, M=512.15 [g/mol]

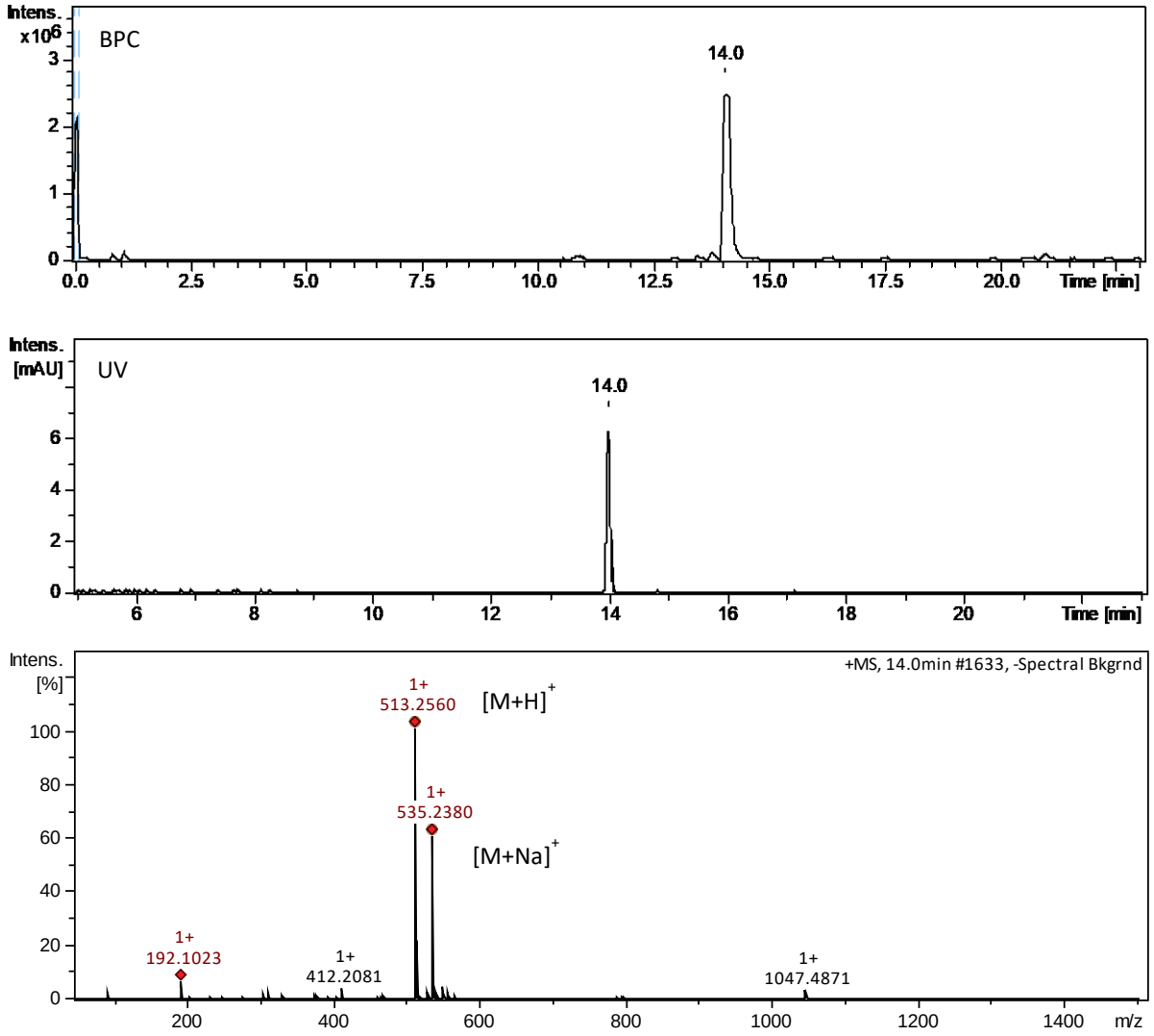

Figure S29. LC-MS characterization of crude Bz-ABBA. The main signal corresponds to the product **OU7**. It appears in the spectrum in the form of two adducts: $[M+H]^+$ (m/z=513.2560) and $[M+Na]^+$ (m/z=535.2380).

OU8

Bz-BABA, M=512.15 [g/mol]

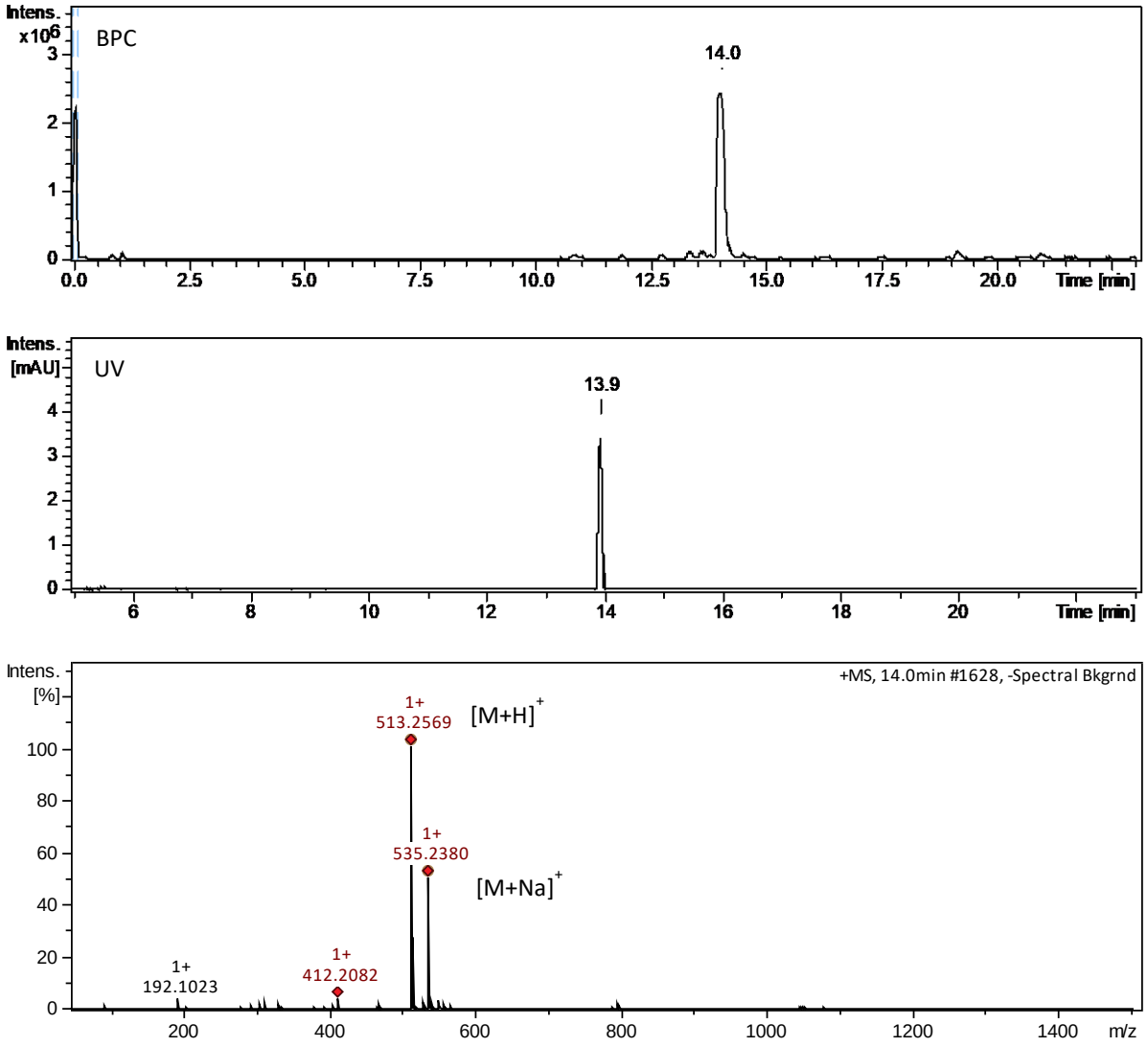

Figure S30. LC-MS characterization of crude Bz-BABA. The main signal corresponds to the product **OU8**. It appears in the spectrum in the form of two adducts: $[M+H]^+$ (m/z=513.2569) and $[M+Na]^+$ (m/z=535.2380).

OU9

Bz-ACAA, M=574.62 [g/mol]

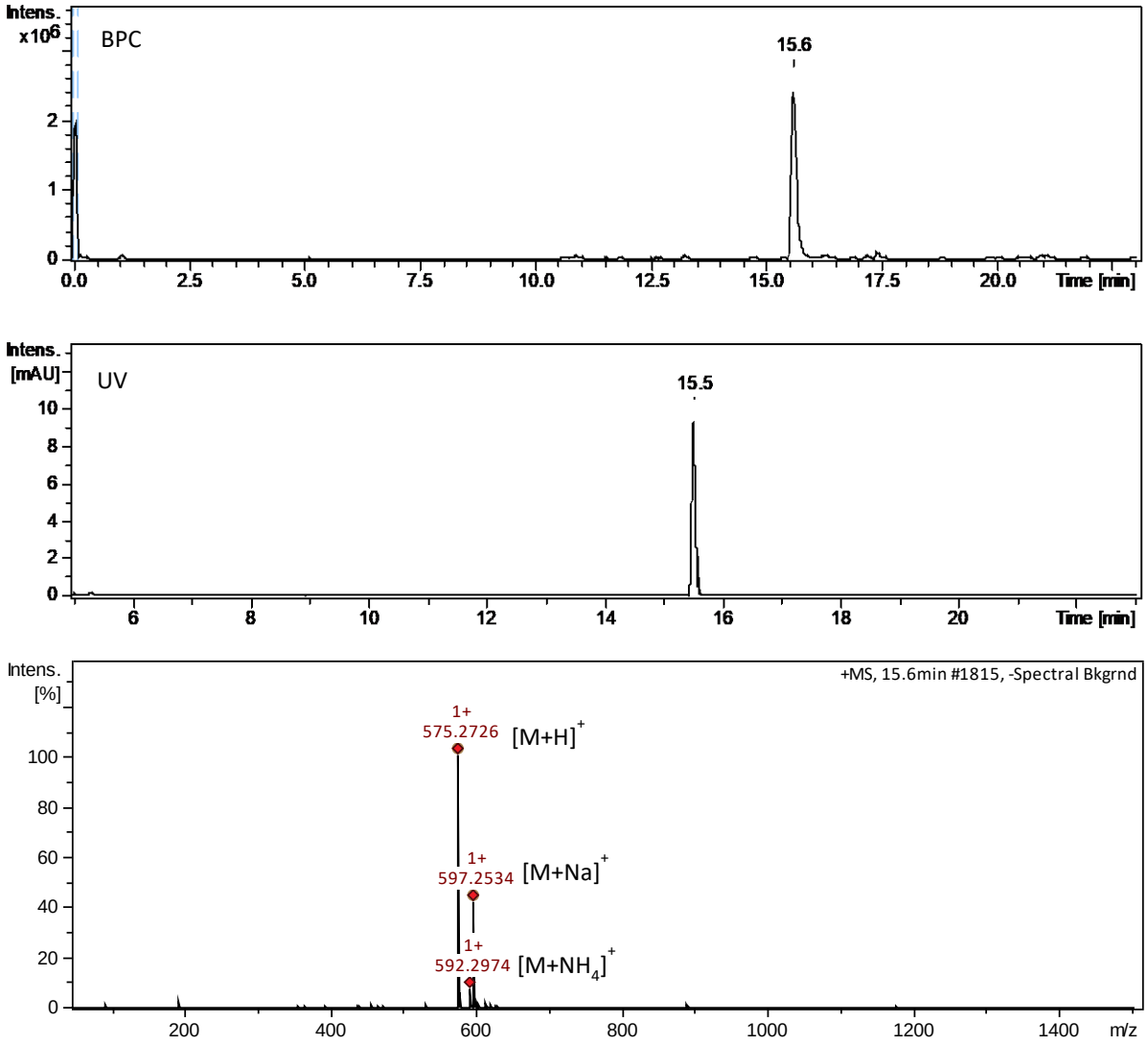

Figure S31. LC-MS characterization of crude Bz-ACAA. The main signal corresponds to the product **OU9**. It appears in the spectrum in the form of three adducts: $[M+H]^+$ (m/z=575.2726), $[M+Na]^+$ (m/z=597.2534) and $[M+NH_4]$ (m/z=592.2974).

OU10

Bz-CBCC, M=698.76 [g/mol]

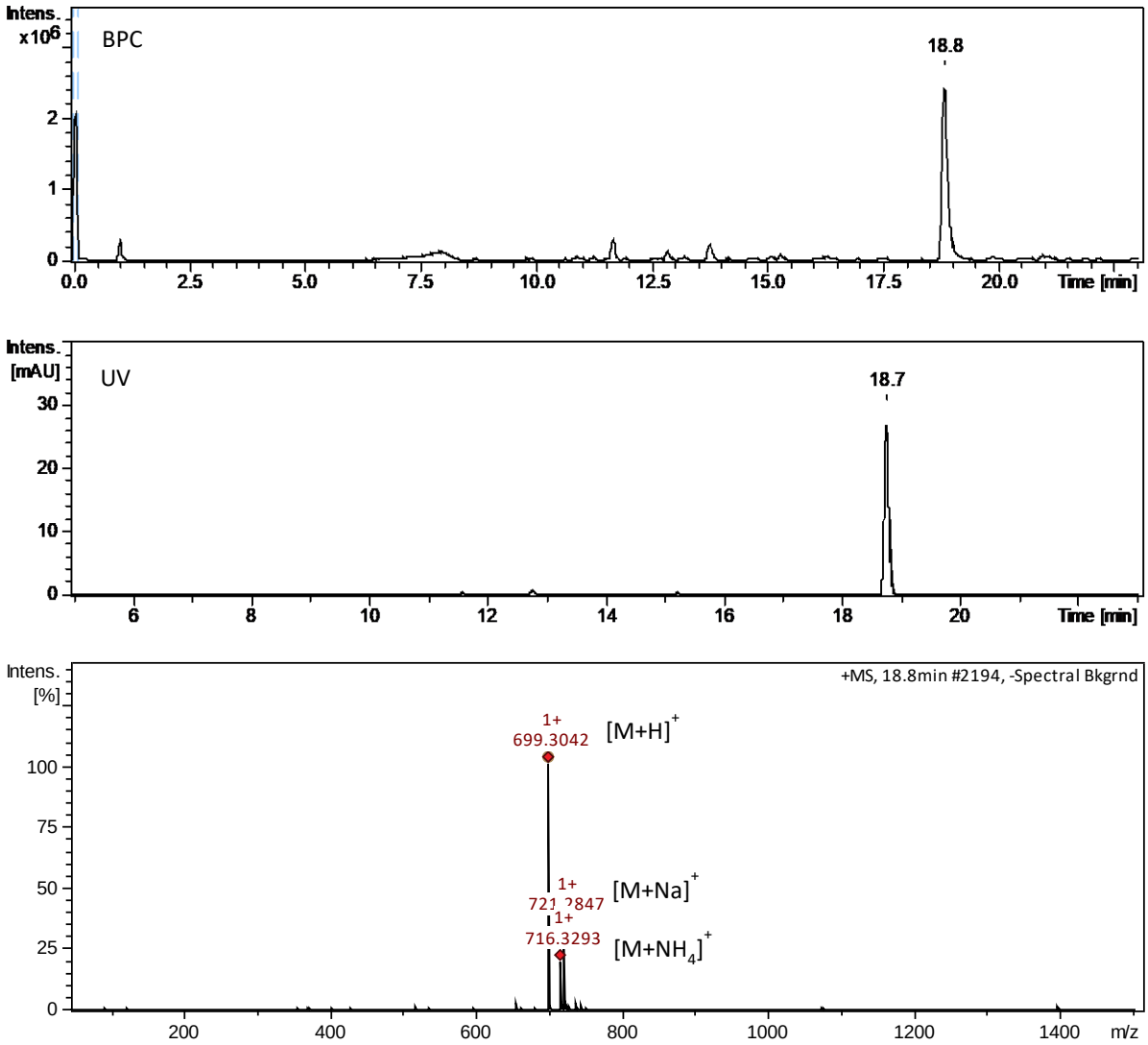

Figure S32. LC-MS characterization of crude Bz-CBCC. The main signal corresponds to the product **OU10**. It appears in the spectrum in the form of three adducts: $[M+H]^+$ (m/z=699.3042), $[M+Na]^+$ (m/z=721.7847) and $[M+NH_4]$ (m/z=716.3293).

E. Circular Dichroism (CD)

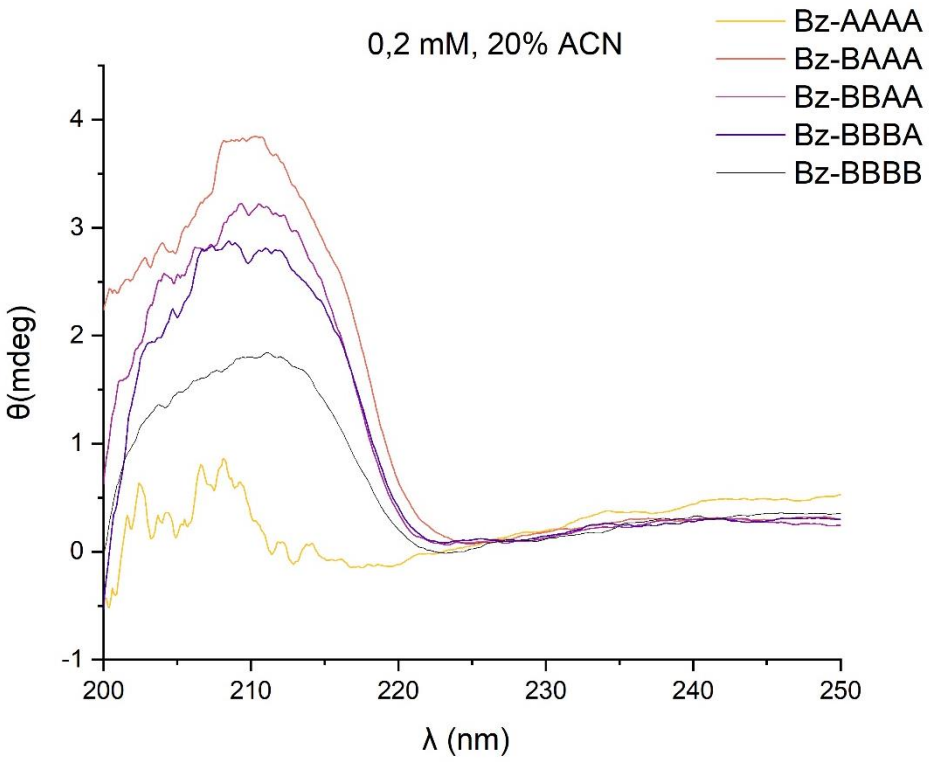

Figure S33. CD of oligomers OU1, OU2, OU4, OU5 and OU6 measured in 20% ACN in water.

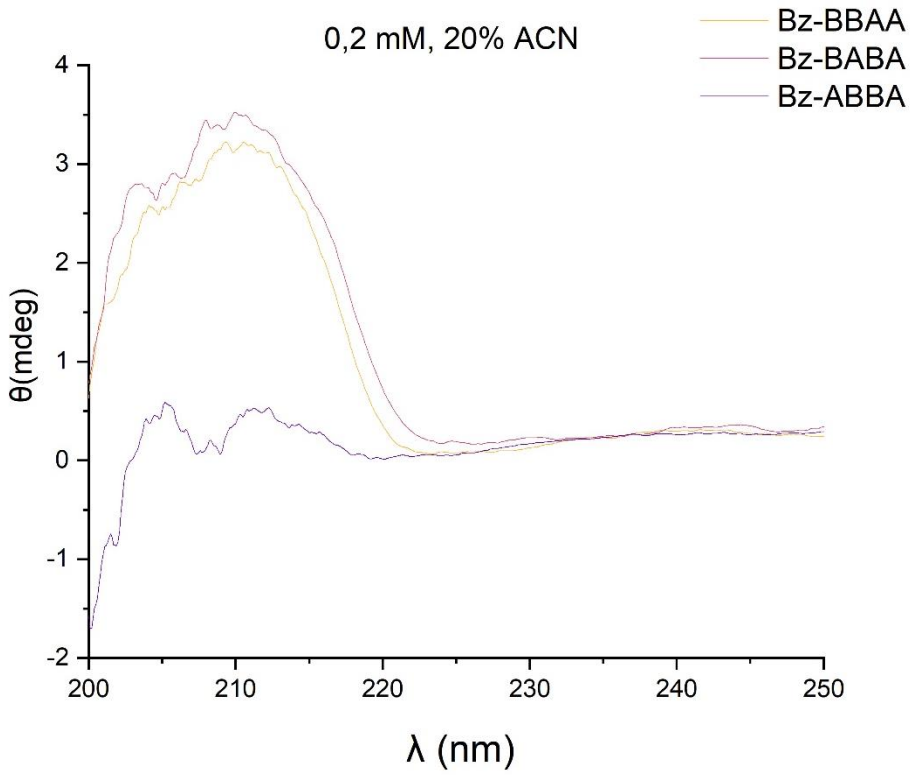

Figure S34. CD of oligomers OU4, OU7, and OU8 measured in 20% ACN in water.

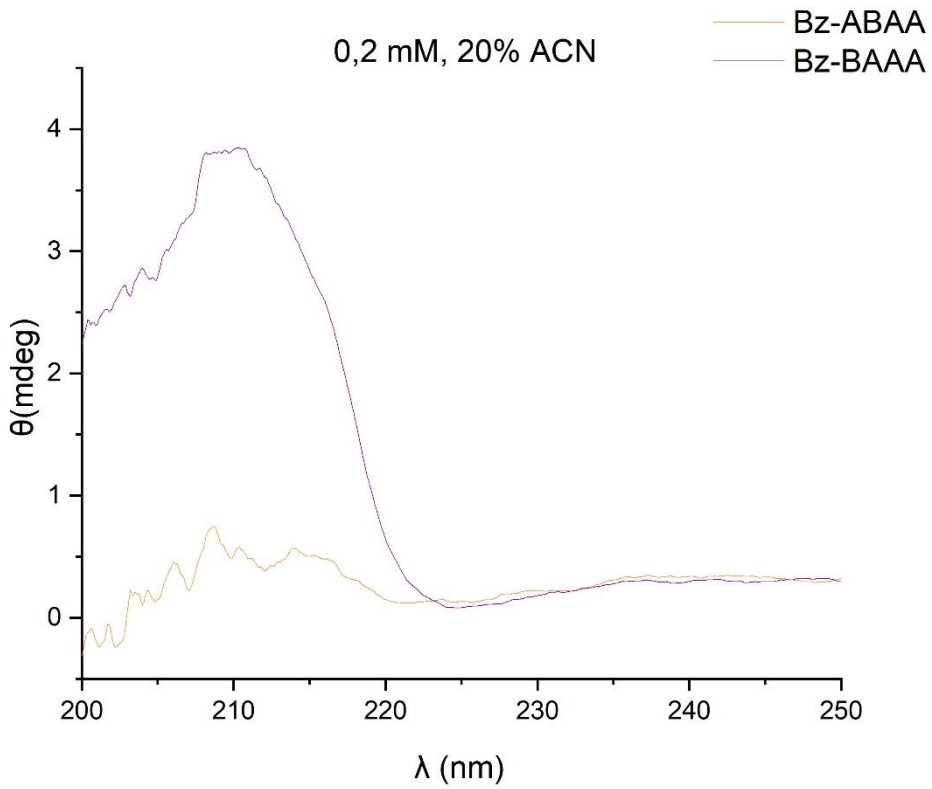

Figure S35. CD of oligomers OU2 and OU3 measured in 20% ACN in water.

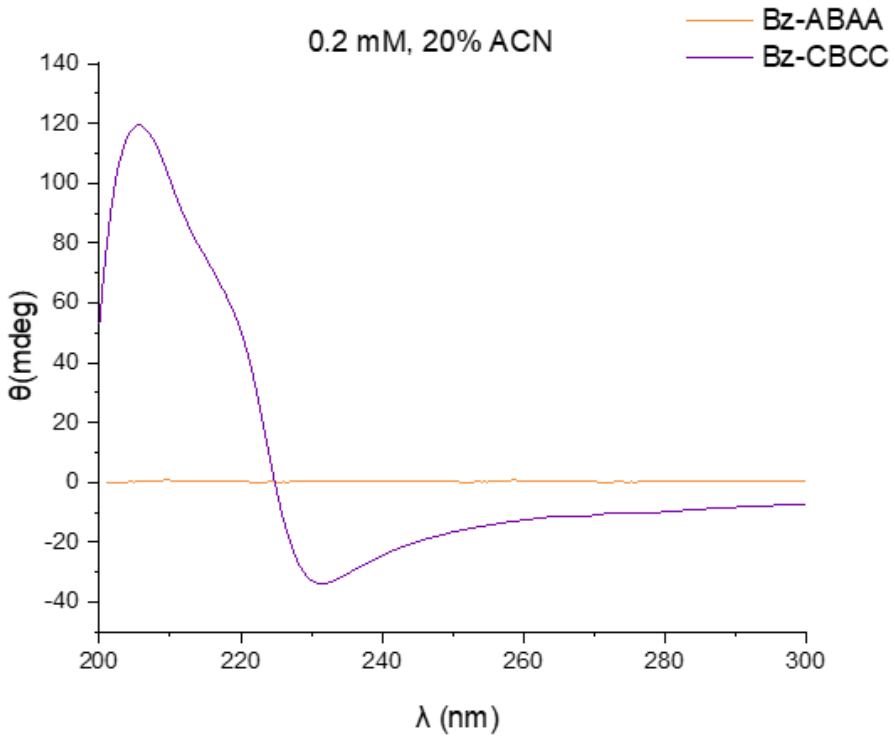

Figure S36. CD of oligomers OU3 and OU10 measured in 20% ACN in water.

Table S4. Ellipticity and molar ellipticity values for oligomers with the chiral center.

Oligomer	Sequence	Θ [mdeg][a]	[θ] [deg×cm^2/dmol][b]
OU2	Bz-BAAA	3.85	3845.34
OU3	Bz-ABAA	0.75	748.61
OU4	Bz-BBAA	3.22	3221.80
OU5	Bz-BBBA	2.88	2878.56
OU6	Bz-BBBB	1.84	1842.75
OU7	Bz-ABBA	0.59	588.51
OU8	Bz-BABA	3.52	3522.97
OU10	Bz-CBCC	119.37	162740.47

[a] Ellipticity determined experimentally from CD measurements; [b] Molar ellipticity, calculated from ellipticity, $[\theta] = \frac{\Theta \times \mathrm{M}}{10 \times L \times C}$, where M is molar mass (g/mol), L is path length of cell (cm) and C is concentration (g/L).

F. Differential Scanning Calorimetry (DSC)

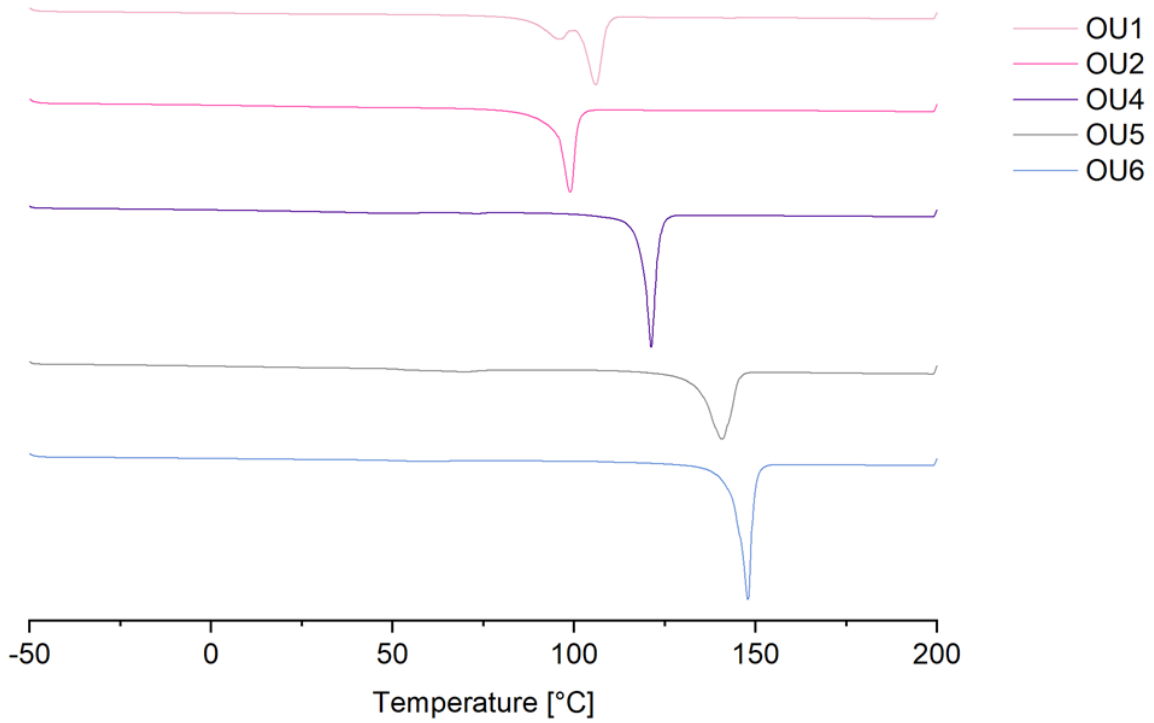

Figure S37. The first cycle of heating DSC curves of Bz-AAAA, Bz-BAAA, Bz-BBAA, Bz-BBBA and Bz-BBBB.

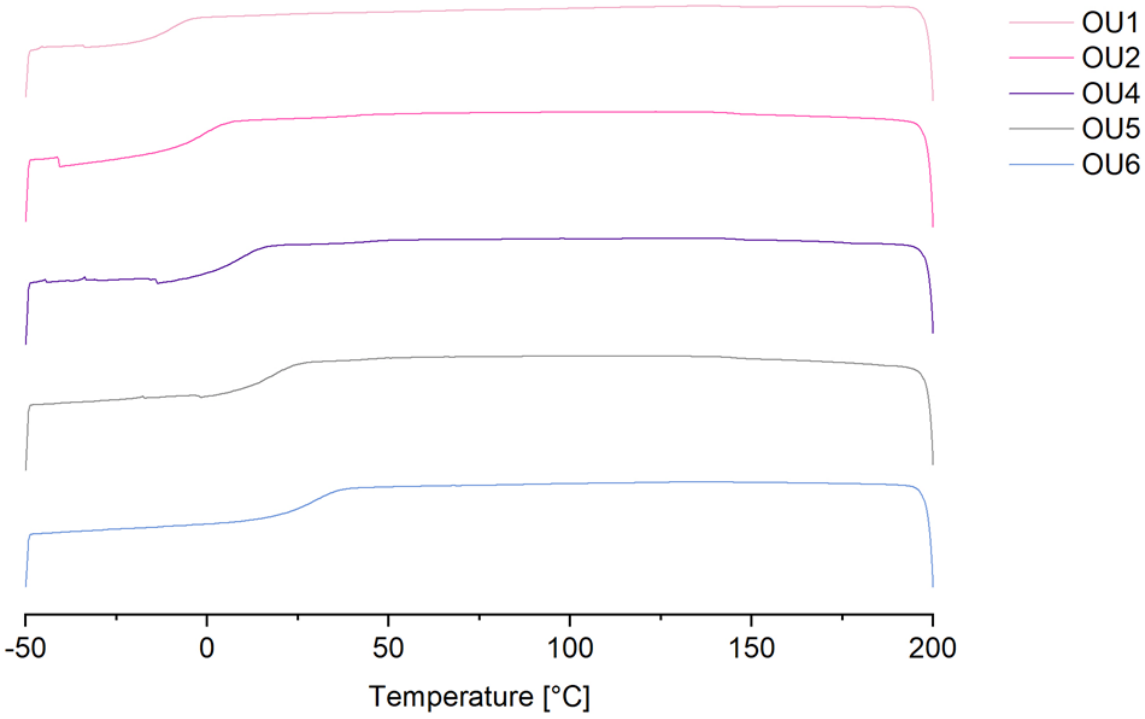

Figure S38. Cooling DSC curves of Bz-AAAA, Bz-BAAA, Bz-BBAA, Bz-BBBA and Bz-BBBB.

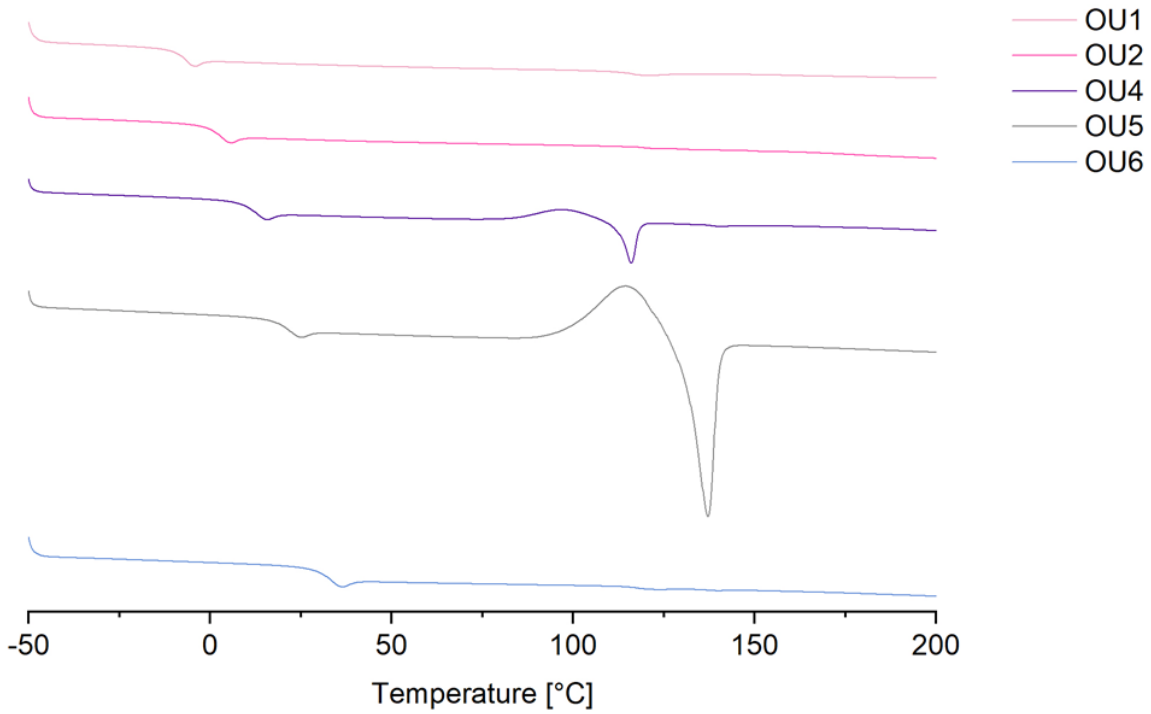

Figure S39. The second cycle of heating DSC curves of Bz-AAAA, Bz-BAAA, Bz-BBAA, Bz-BBBA and Bz-BBBB.

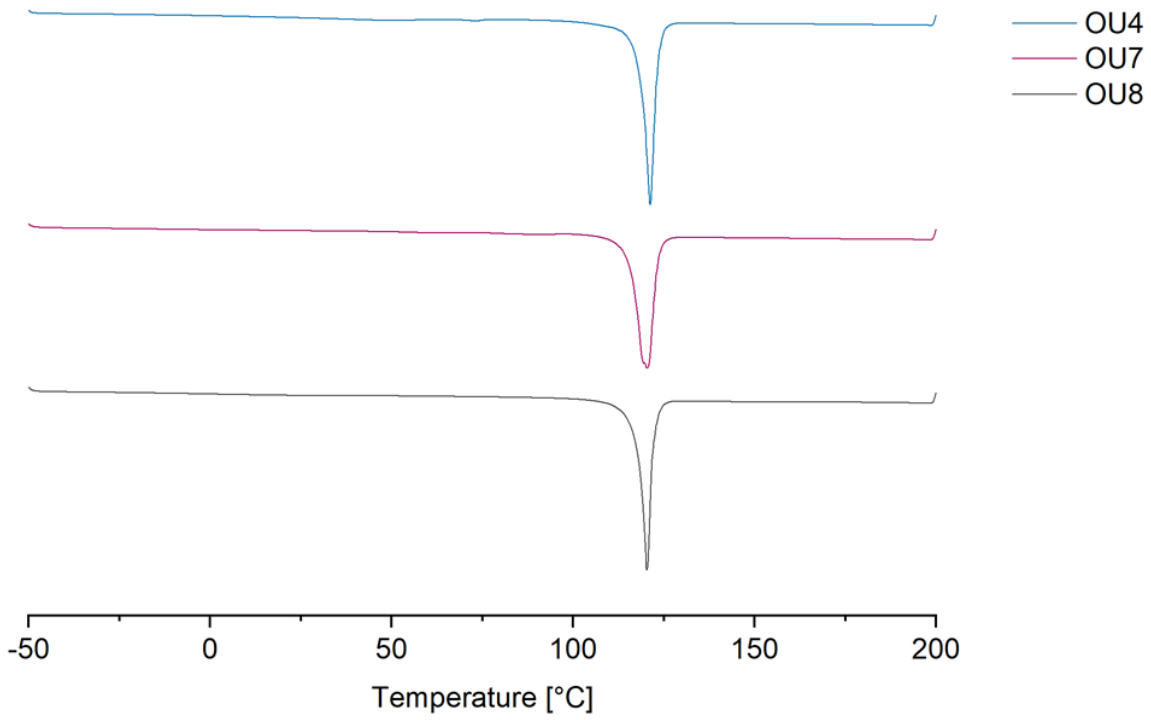

Figure S40. The first cycle of heating DSC curves of Bz-BBAA, Bz-ABBA, and Bz-BABA.

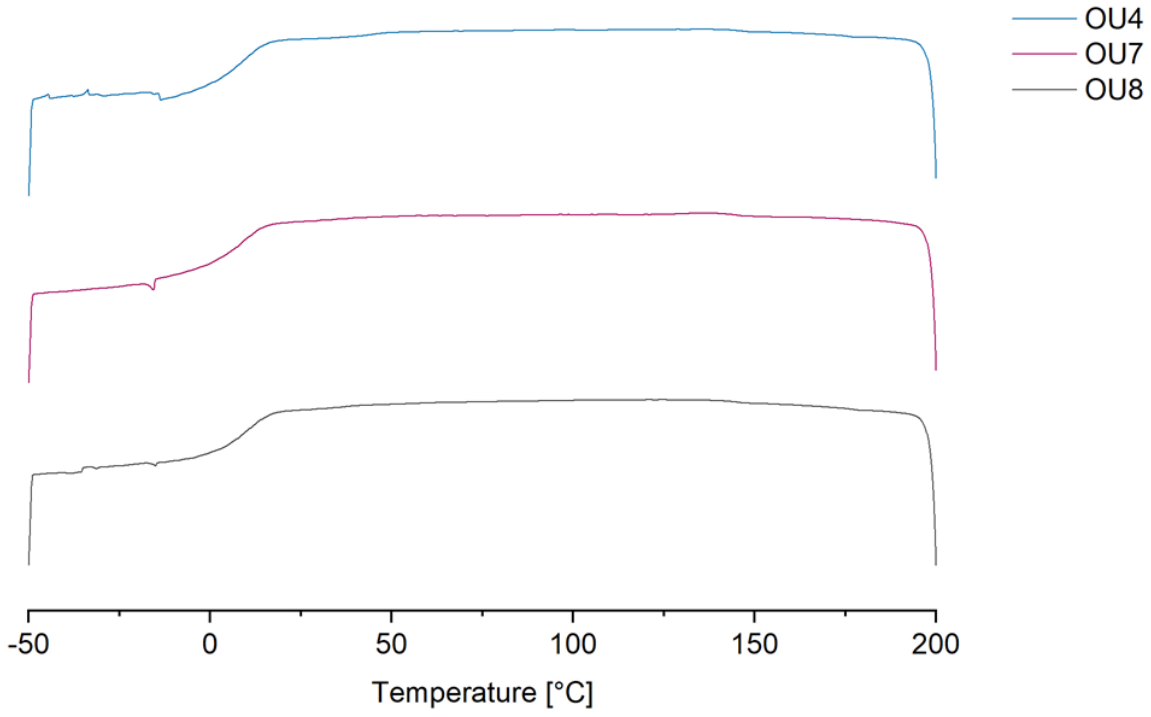

Figure S41. Cooling DSC curves of Bz-BBAA, Bz-ABBA, and Bz-BABA.

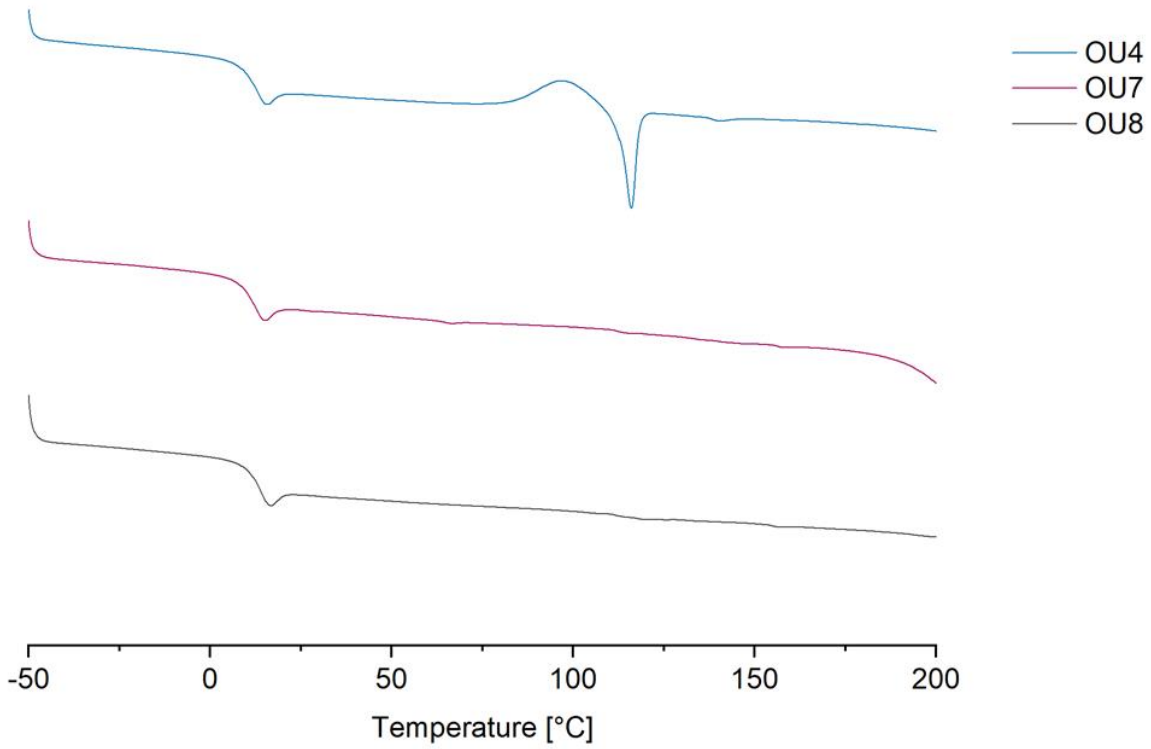

Figure S42. The second cycle of heating DSC curves of Bz-BBAA, Bz-ABBA, and Bz-BABA.

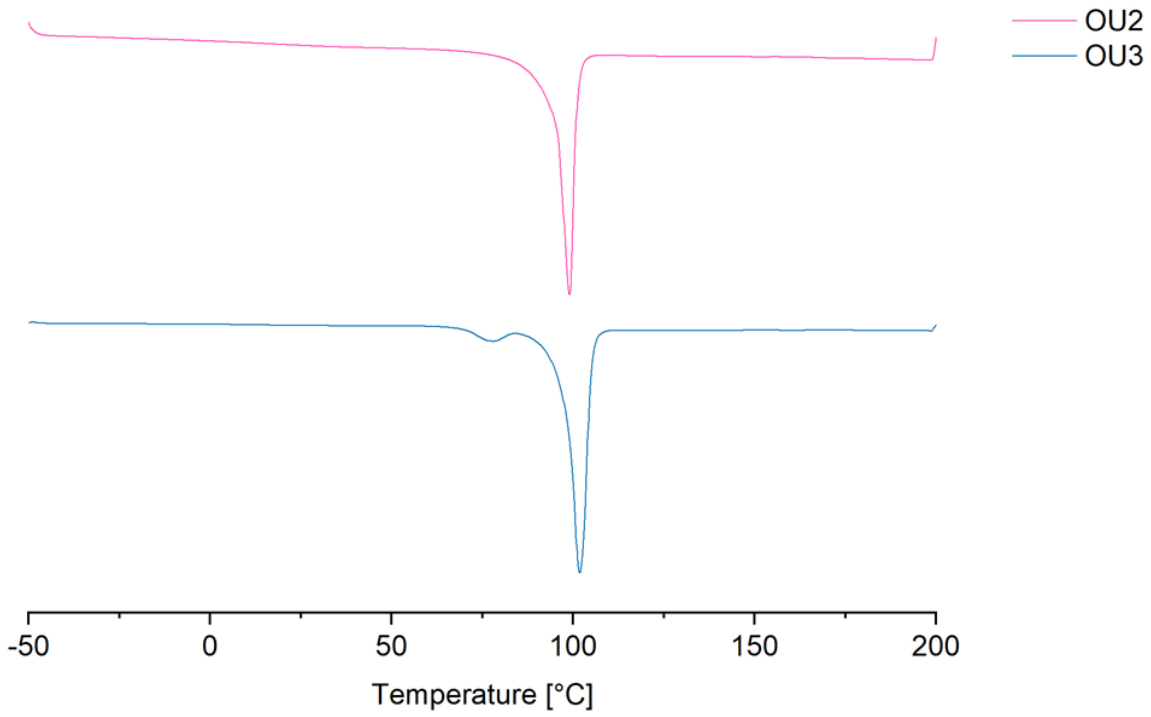

Figure S43. The first cycle of heating DSC curves of Bz-BAAA and Bz-ABAA.

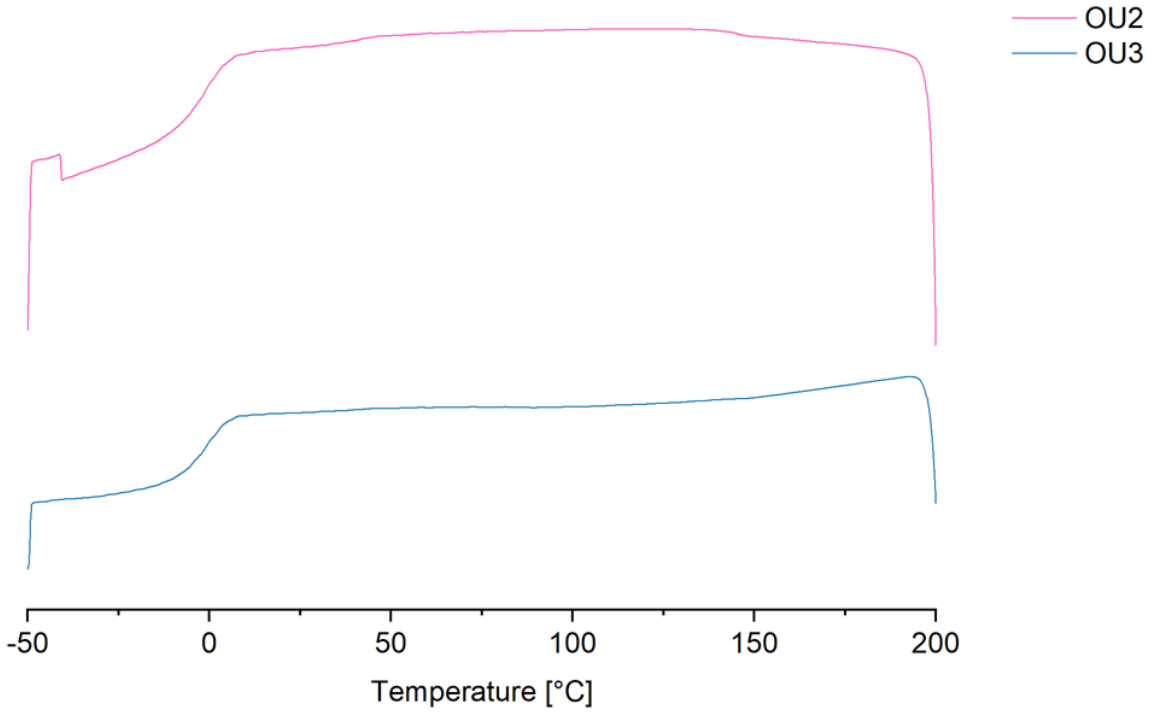

Figure S44. Cooling DSC curves of Bz-BAAA and Bz-ABAA.

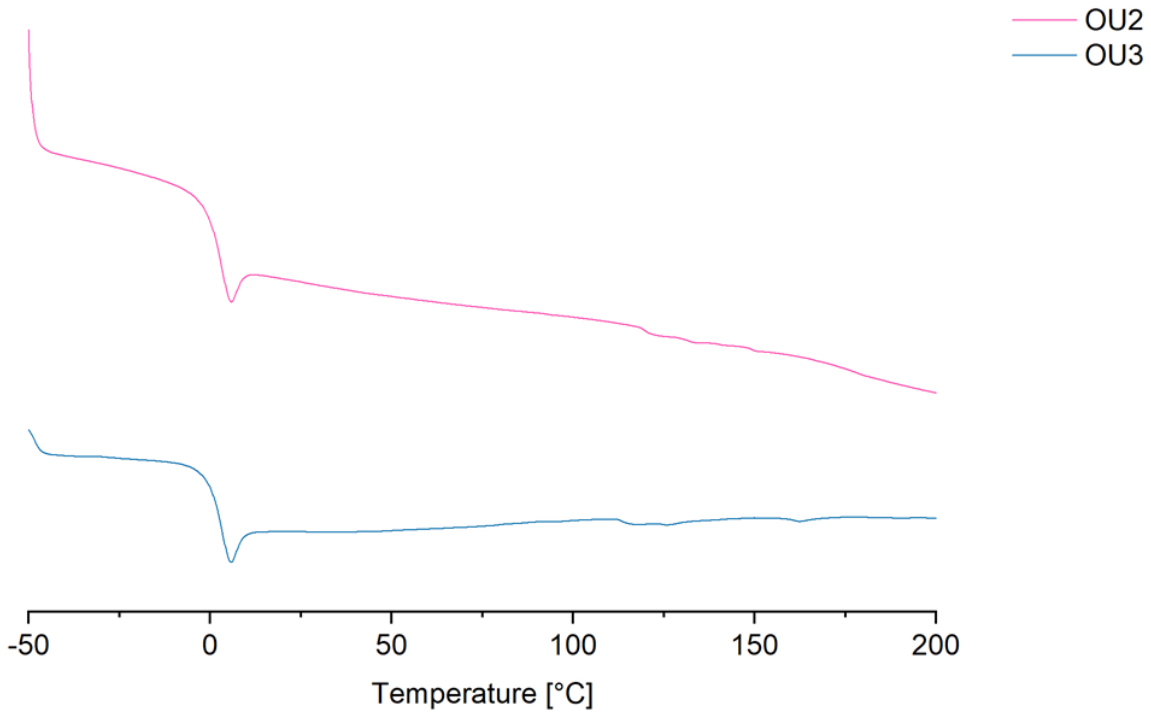

Figure S45. The second cycle of heating DSC curves of Bz-BAAA and Bz-ABAA.

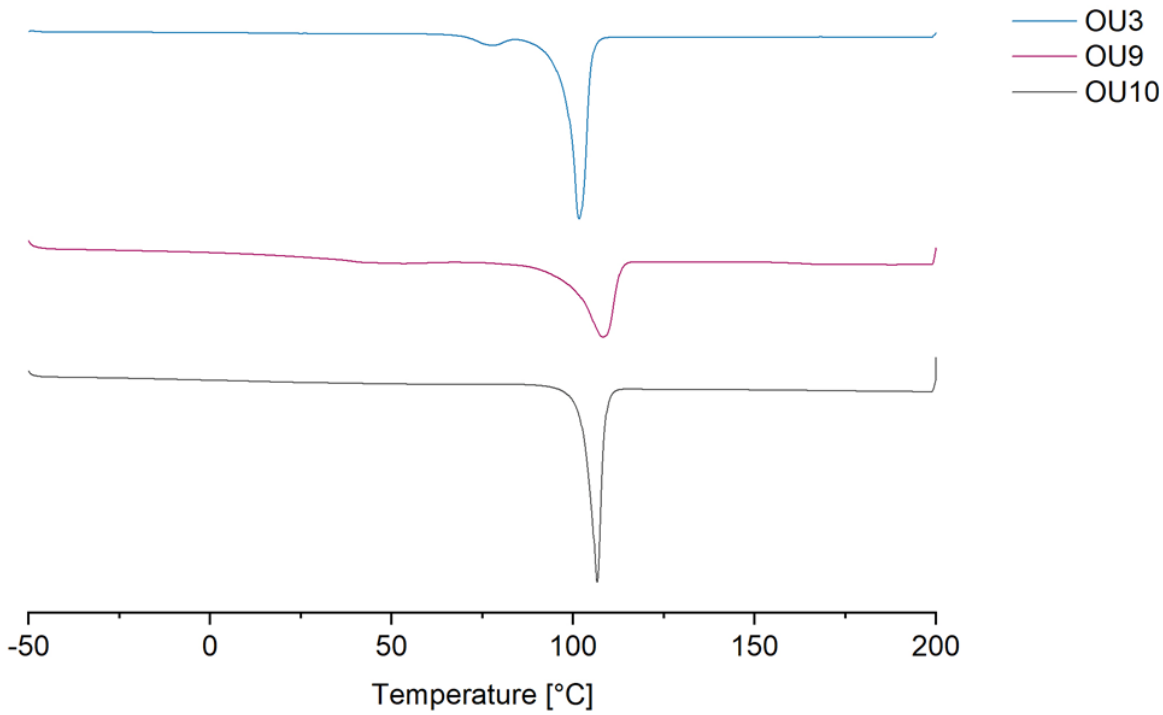

Figure S46. The first cycle of heating DSC curves of Bz-ABAA, Bz-ACAA, and Bz-CBCC.

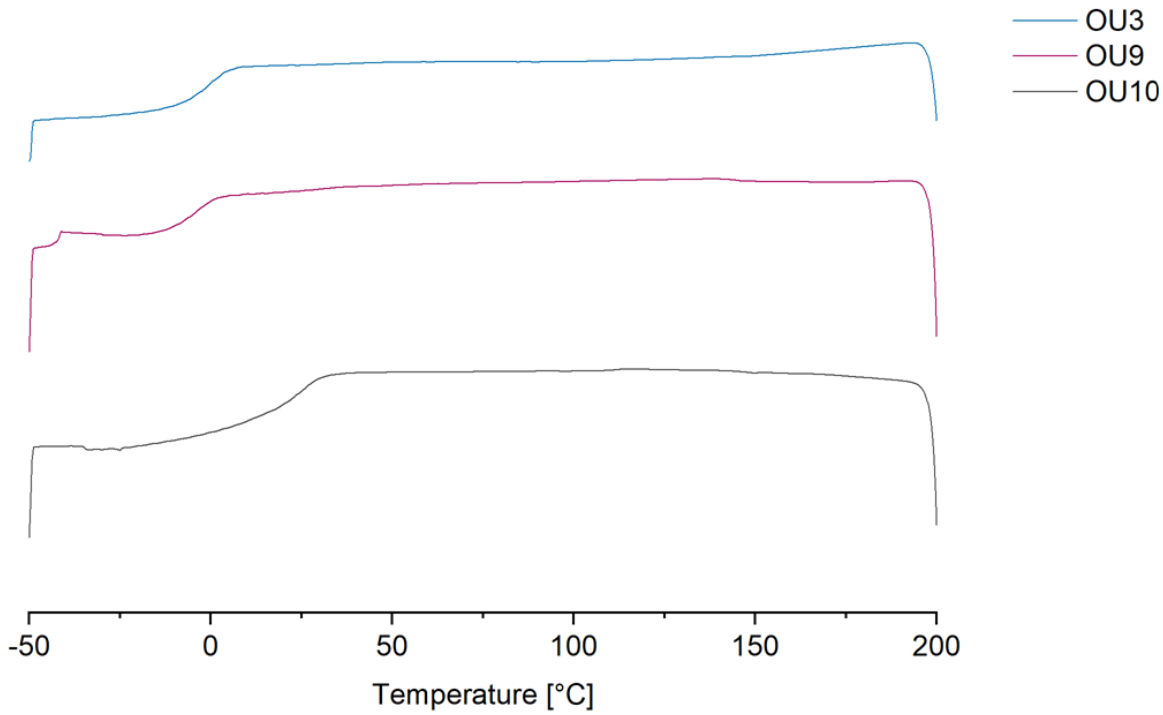

Figure S47. Cooling DSC curves of Bz-ABAA, Bz-ACAA, and Bz-CBCC.

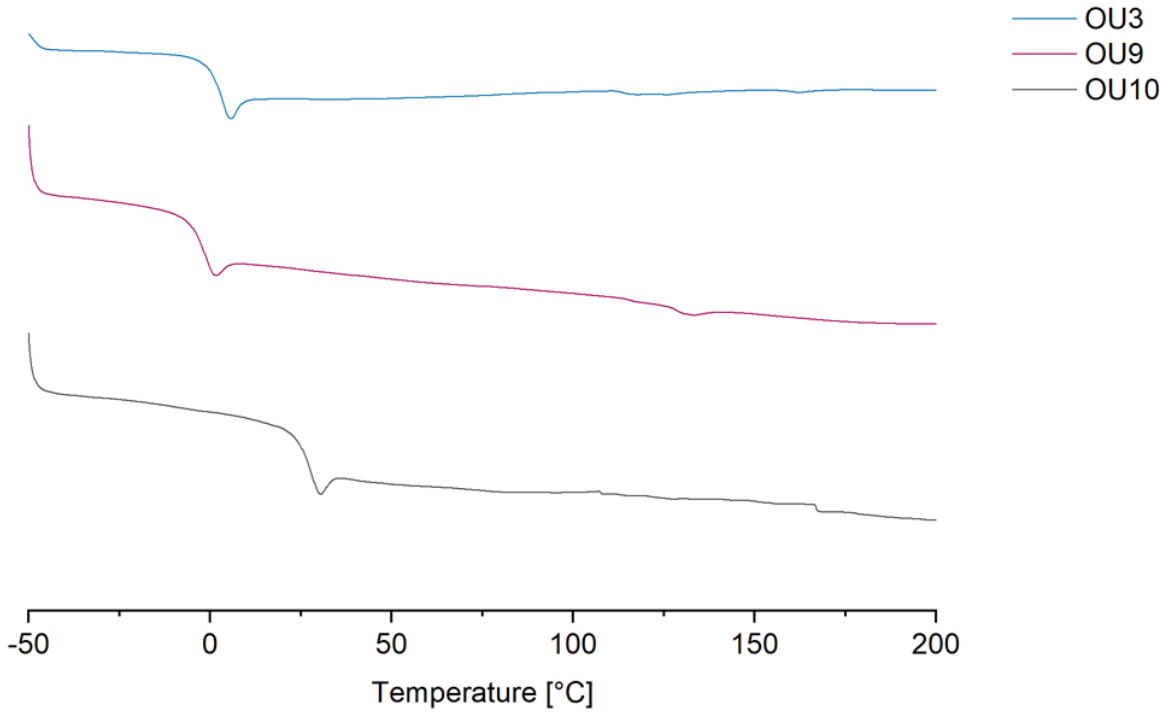

Figure S48. The second cycle of heating DSC curves of Bz-ABAA, Bz-ACAA, and Bz-CBCC.

G. Thermogravimetric Analysis (TGA)

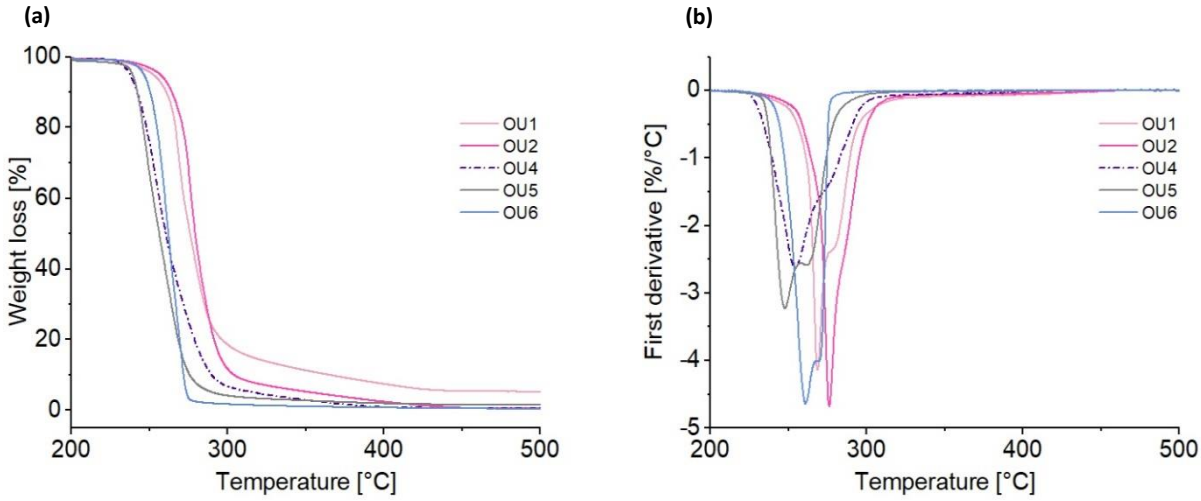

Figure S49. Comparison of TGA thermograms (a) and DTGA graphs (b) for oligomers of Bz-AAAA, Bz-BAAA, Bz-BBAA, Bz-BBBA and Bz-BBBB.

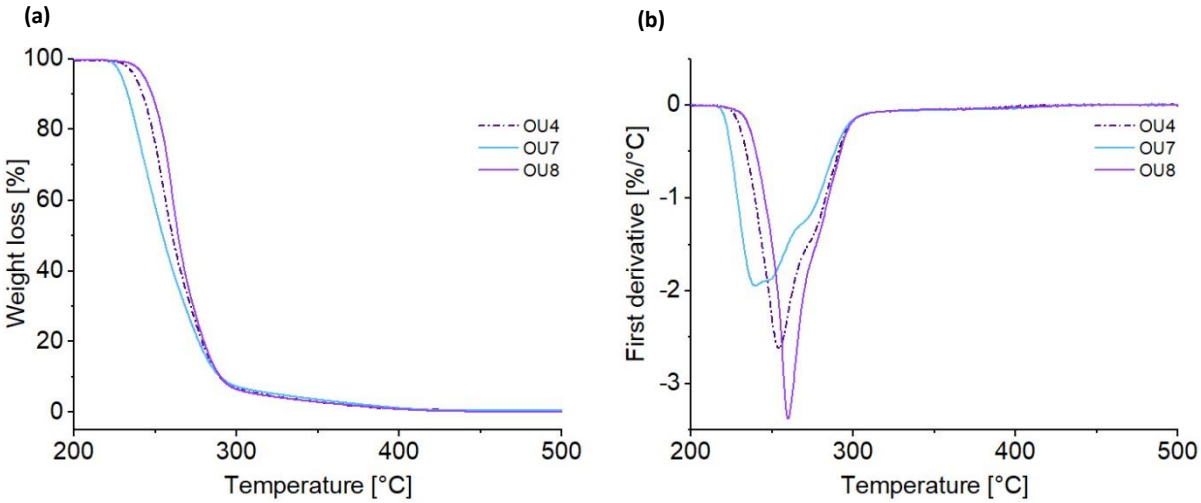

Figure S50. Comparison of TGA thermograms (a) and DTGA graphs (b) for oligomers Bz-BBAA, Bz-ABBA and Bz-BABA.

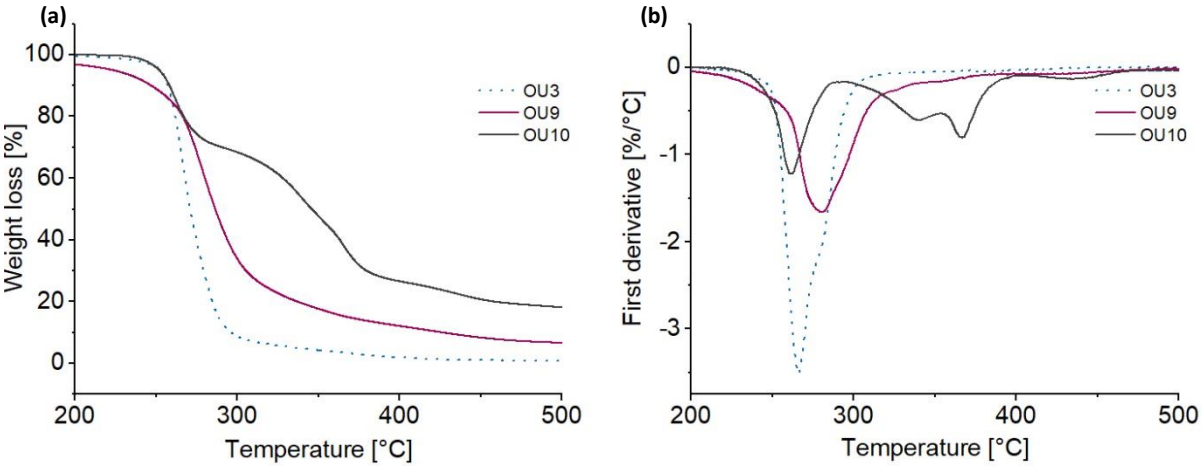

Figure S51. Comparison of TGA thermograms (a) and DTGA graphs (b) for oligomers Bz-ABAA, Bz-ACAA and Bz-CBCC.

H. Urethane Degradation

1. Mechanism

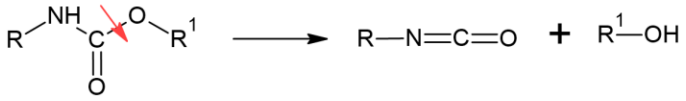

2. Mechanism

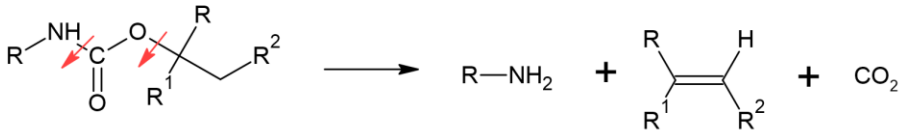

3. Mechanism

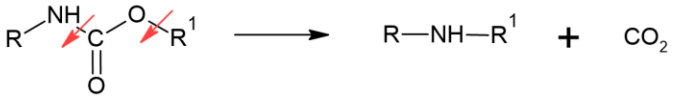

Figure S52. Three possible pathways of urethane linkages thermal degradation.[3]

I. Fourier transform infrared spectroscopy (FTIR)

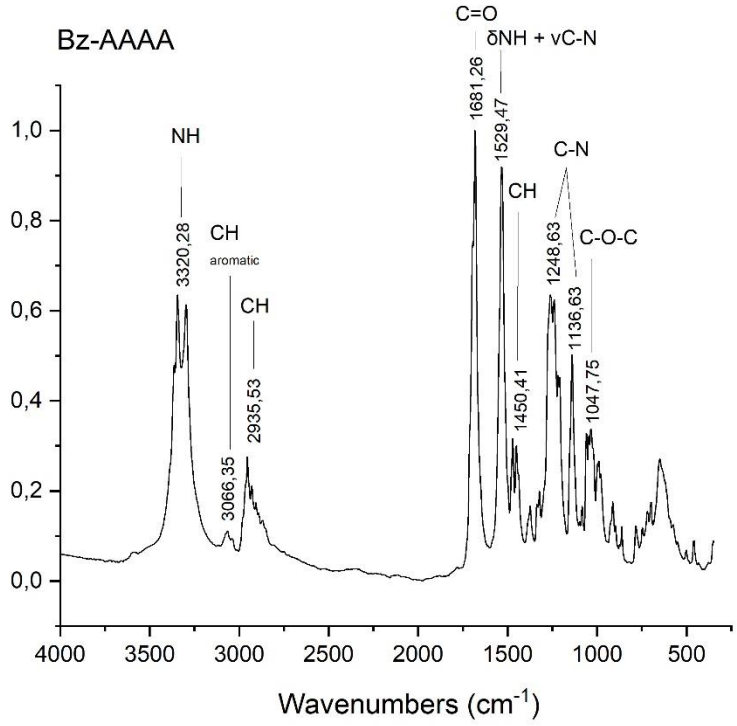

Figure S53. IR spectrum of oligomer **OU1** Bz-AAAA.

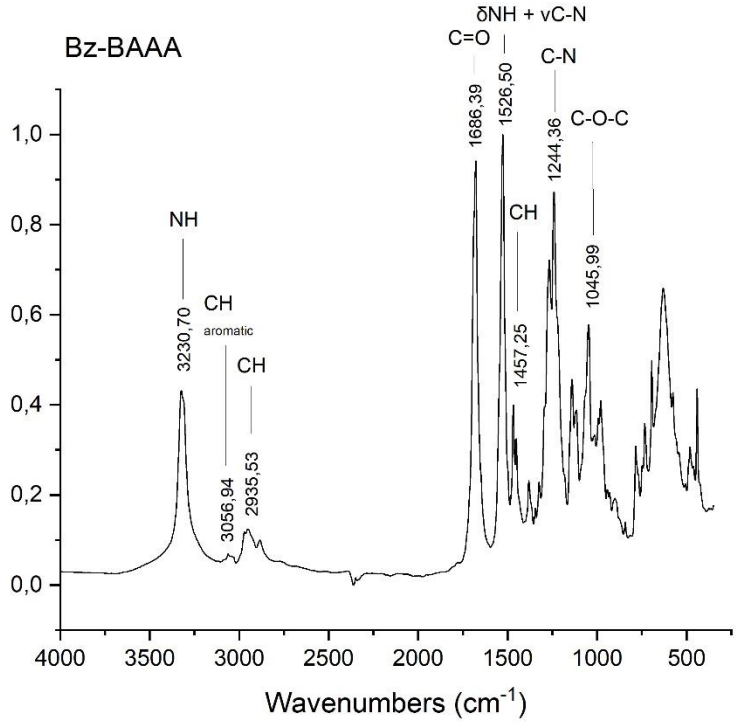

Figure S54. IR spectrum of oligomer **OU2** Bz-BAAA.

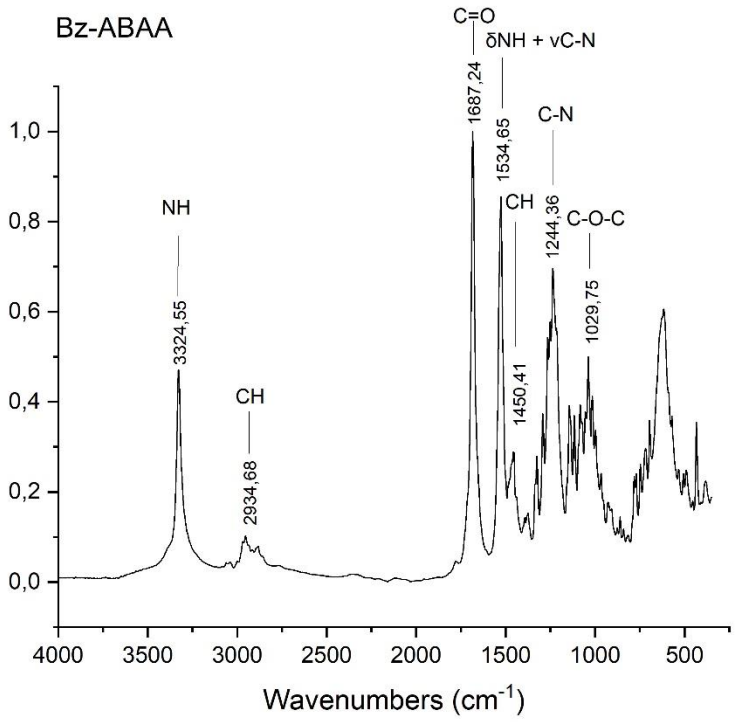

Figure S55. IR spectrum of oligomer **OU3** Bz-ABAA.

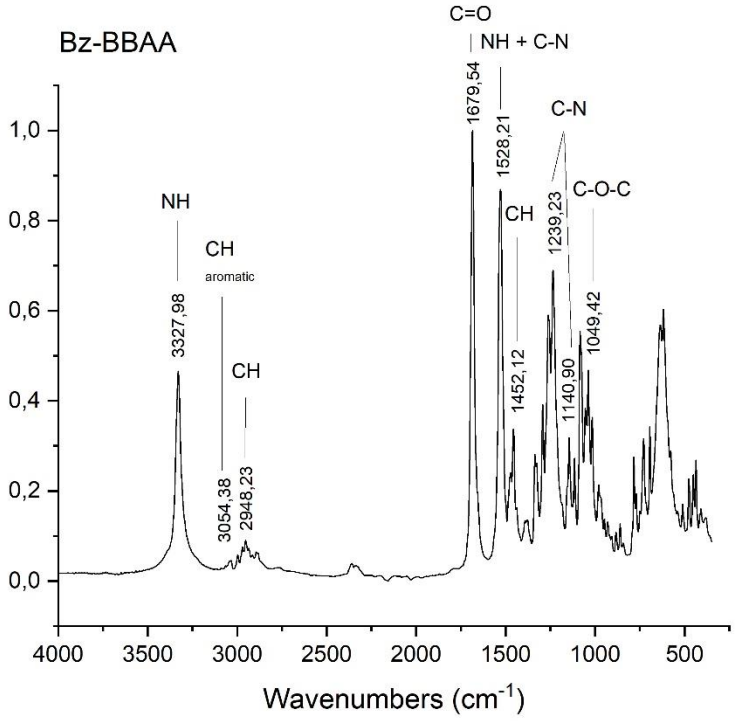

Figure S56. IR spectrum of oligomer **OU4** Bz-BBAA.

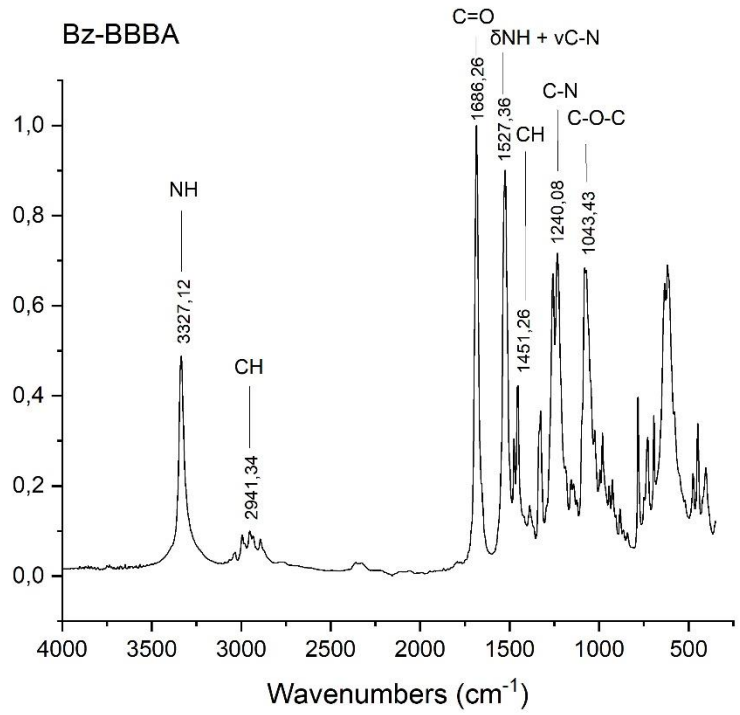

Figure S57. IR spectrum of oligomer **OU5** Bz-BBBA.

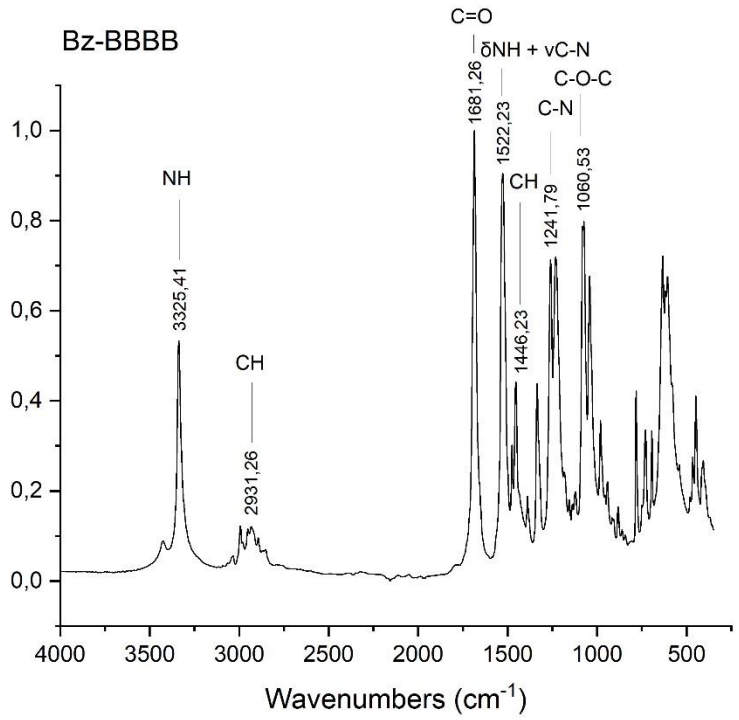

Figure S58. IR spectrum of oligomer **OU6** Bz-BBBB.

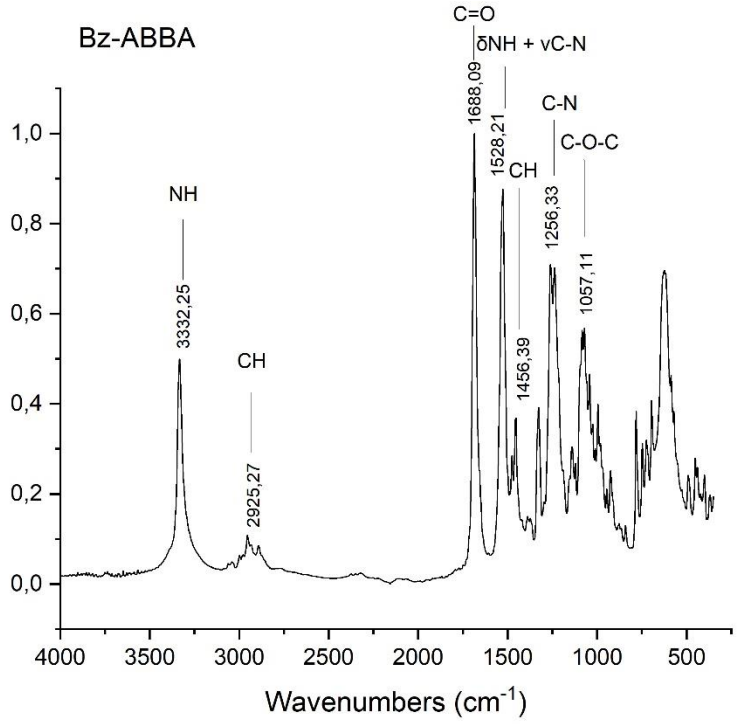

Figure S59. IR spectrum of oligomer **OU7** Bz-ABBA.

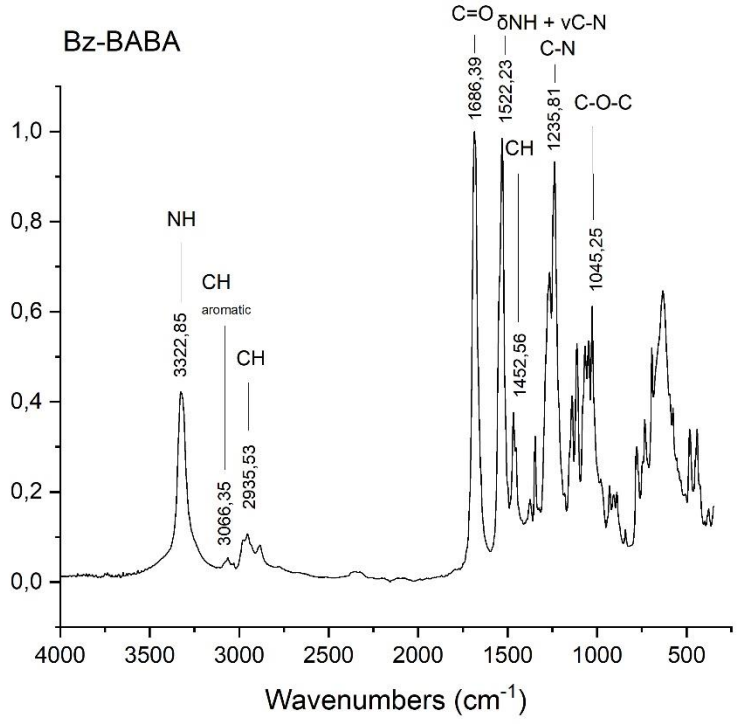

Figure S60. IR spectrum of oligomer **OU8** Bz-BABA.

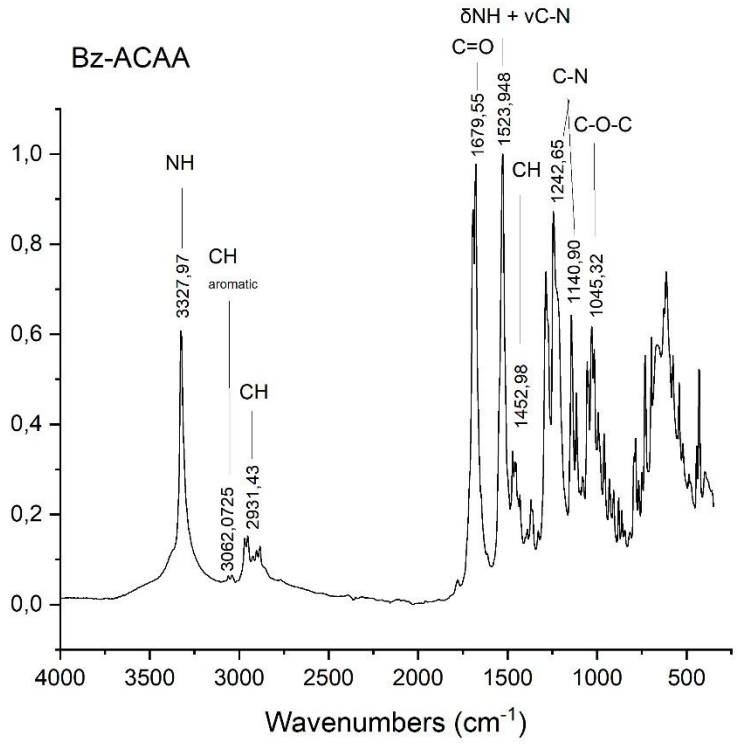

Figure S61. IR spectrum of oligomer **OU9** Bz-ACAA.

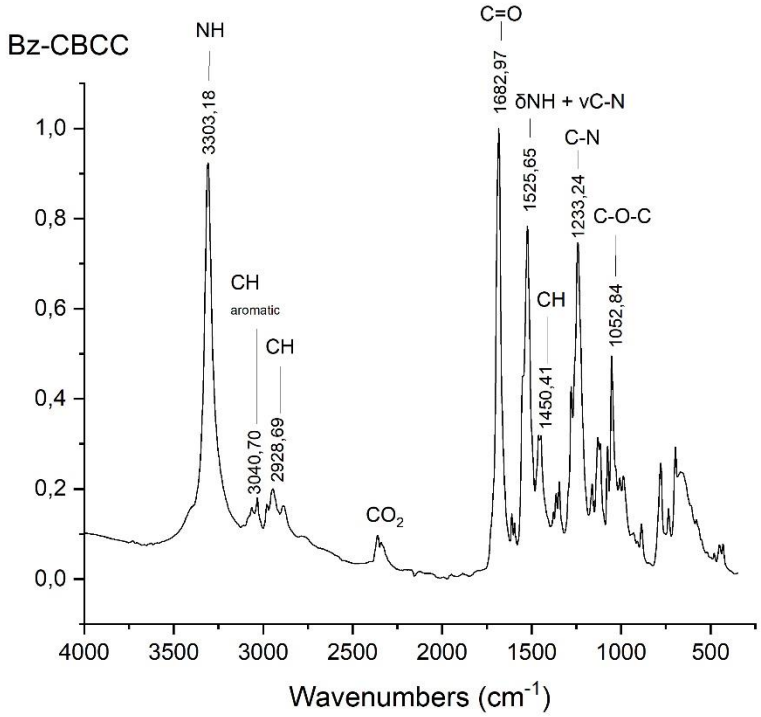

Figure S62. IR spectrum of oligomer **OU10** Bz-CBCC.

J. Gram–Schmidt curves

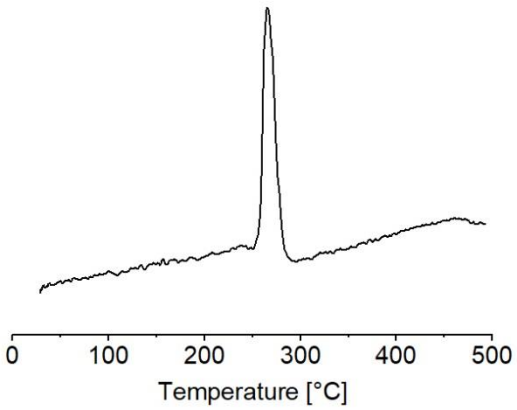

Figure S63. Gram–Schmidt of oligomer **OU1** Bz-AAAA.

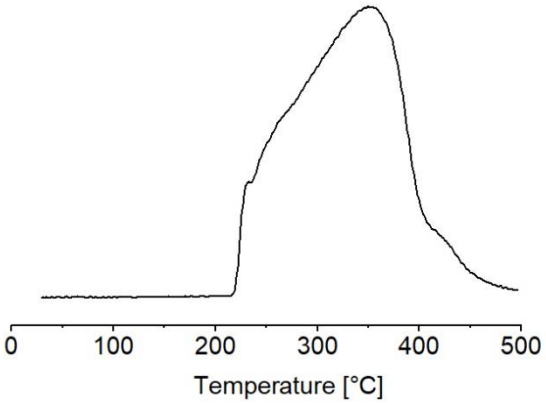

Figure S64. Gram–Schmidt of oligomer **OU5** Bz-BBBA.

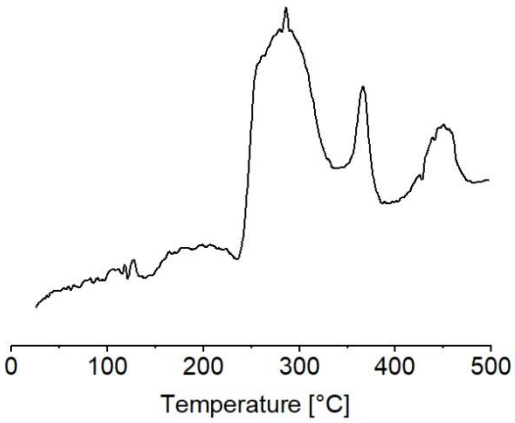

Figure S65. Gram–Schmidt of oligomer **OU10** Bz-CBCC.

K. Analysis of degradation products

Table S5. Assignements of IR signals for OU1, OU5 and OU10.

Bz-AAAA **OU1 (cm^{-1})**	**Bz-BBBA** **OU5 (cm^{-1})**	**Bz-CBCC** **OU10 (cm^{-1})**	**Assignement**
3343	3327	3303	*v*N-H
3052	3039	3040	*v*C-H aromatic
2931	2941	2928	*v*C-H aliphatic
1684	1686	1683	*v*C=O
1534	1527	1525	*v*C-N, δN-H
1262	1240	1233	*v*C-N
1047	1043	1052	*v*C-O-C
	Degradation products		
	3487		*v*H-N-H
3229		3233	*v*OH
3090	3075	3078	*v*C=CH
2720	2732	2728	*v*C-CH
	1822	1822	*v*C=O (α-lactones)
1780			*v*C=O (γ-lactones)
1729		1729	*v*C=O (unsaturated and aryl esters)
1379	1385	1383	*v*C=CH
1198	1201	1205	*v*C=CH
1020	1024	1024	δC=CH

Red: Signals that appeared at the temperature at the first maximum of the Gram- Schmidt curves; blue: signals appeared at the temperatures for which the most significant structural differences in spectra were observed.

L. Melting point calculations

Table S6. Melting point calculations based on van Krevelen additive group theory.

Sequence	Y_M value [K kg mol^{-1}59]	T_m [°C]
Bz-AAAA OU1	242	199.7
Bz-BAAA OU2	251	217.2
Bz-ABAA OU3	251	217.2
Bz-BBAA OU4	260	234.8
Bz-BBBA OU5	269	252.4
Bz-BBBB OU6	278	270.0
Bz-ABBA OU7	260	234.8
Bz-BABA OU8	260	234.8
Bz-ACAA OU9	286	224.7
Bz-CBCC OU10	383	275.1

First Y_M was calculated from additive group theory[4], afterwards T_m in Kelvins was calculated from the equation $T_m = \frac{\sum_i Y_{mi} \times 10^3}{M}$. Than Kelvins were transformed to Celsius degrees.

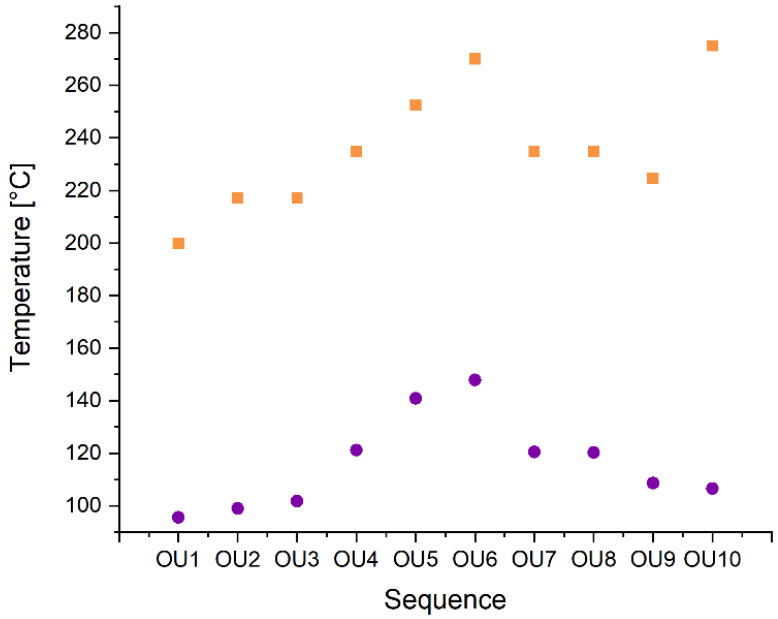

Figure S66. Comparison of the melting points determined experimentally from the DSC measurement (●) and the calculated (▪) using the method of van Krevelen. The experimental melting temperatures are about 100 °C lower than experimental T_m values, however, the trend is matching.

M. Gel permeation chromatography - M_p calculations

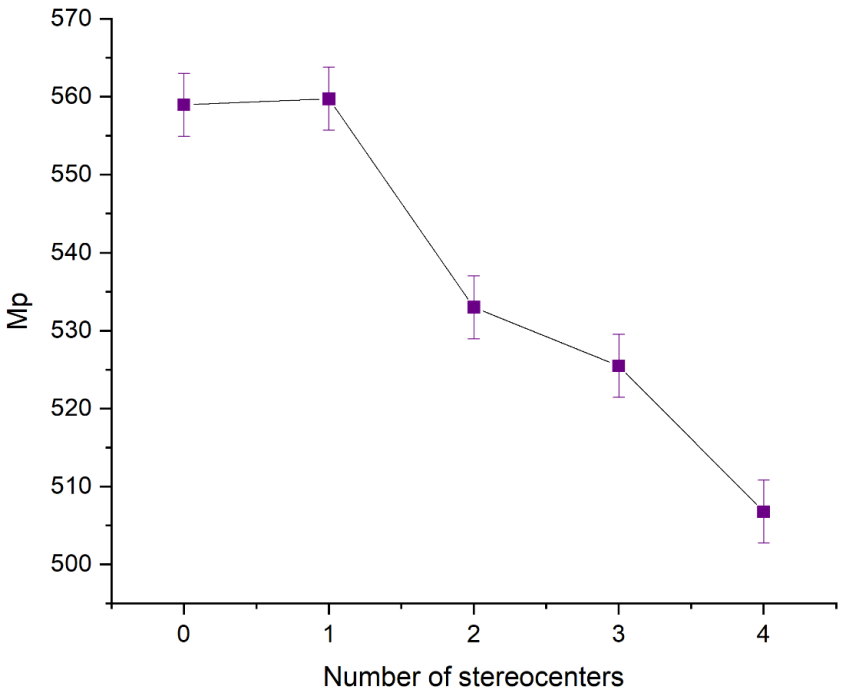

Figure S67. Realation between the number of chiral units and mass in maximum of peak determined by GPC. The error was calculated for three representative samples based on three independent mesurement using the formula for standard deviation: $\sigma = \sqrt{\frac{\sum_{i=1}^{n}(x_i - x)^2}{n-1}}$, where x_i is a data point, x is the mean and n is a number of data points.

IV. References

[1] E. B. Stopler, O. J. Dodo, A. C. Hull, K. A. Weaver, P. Chakma, R. Edelmann, L. Ranly, M. B. Zanjani, Z. Ye, D. Konkolewicz, *Mater. Adv.* **2020**, *1*, 1071–1076.

[2] P. Chakma, S. V. Wanasinghe, C. N. Morley, S. C. Francesconi, K. Saito, J. L. Sparks, D. Konkolewicz, *Macromol. Rapid Commun.* **2021**, *42*, 2100070.

[3] L. Jiao, H. Xiao, Q. Wang, J. Sun, *Polym. Degrad. Stab.* **2013**, *98*, 2687–2696.

[4] D. W. Van Krevelen, K. Te Nijenhuis, *Properties of Polymers Their Correlation with Chemical Structure; Their Numerical Estimation and Prediction from Additive Group Contributions*, Elsevier, **2009**.